Development 138, 2359-2368 (2011) doi:10.1242/dev.060723

A perfusion-independent role of blood vessels in determining branching stereotypy of lung airways

Alon Lazarus[1], Pierre Marie Del-Moral[2], Ohad Ilovich[3], Eyal Mishani[3], David Warburton[2] and Eli Keshet[1,*]

SUMMARY

Blood vessels have been shown to play perfusion-independent roles in organogenesis. Here, we examined whether blood vessels determine branching stereotypy of the mouse lung airways in which coordinated branching of epithelial and vascular tubes culminates in their co-alignment. Using different ablative strategies to eliminate the lung vasculature, both in vivo and in lung explants, we show that proximity to the vasculature is indeed essential for patterning airway branching. Remarkably, although epithelial branching per se proceeded at a nearly normal rate, branching stereotypy was dramatically perturbed following vascular ablation. Specifically, branching events requiring a rotation to change the branching plane were selectively affected. This was evidenced by either the complete absence or the shallow angle of their projections, with both events contributing to an overall flat lung morphology. Vascular ablation also led to a high frequency of ectopic branching. Regain of vascularization fully rescued arrested airway branching and restored normal lung size and its three-dimensional architecture. This role of the vasculature is independent of perfusion, flow or blood-borne substances. Inhibition of normal branching resulting from vascular loss could be explained in part by perturbing the unique spatial expression pattern of the key branching mediator FGF10 and by misregulated expression of the branching regulators *Shh* and sprouty2. Together, these findings uncovered a novel role of the vasculature in organogenesis, namely, determining stereotypy of epithelial branching morphogenesis.

KEY WORDS: Branching morphogenesis, Lung development, Vascular network, Mouse

INTRODUCTION

The past decade has brought about a conceptual shift regarding the role of the vasculature during organogenesis. Traditionally, blood vessels were thought to be an inert network of tubes supplying tissues with nutrients and enabling gas exchange. It is now evident that the vasculature is implicated in the regulation of many processes via direct communication of endothelial cells with adjacent cells (for a review, see Cleaver and Melton, 2003). The perfusion-independent roles of the vasculature that have been uncovered thus far are primarily in early stages of cell fate determination (Lammert et al., 2001; Matsumoto et al., 2001).

A common principle in organogenesis of tubular organs is coordinated branching morphogenesis of epithelial and vascular networks, culminating in their close physical proximity (Lu and Werb, 2008). However, it is not known how this is attained and specifically which roles, if any, the vasculature play in determining the tissue-specific architecture of branched organs. The lung is a prime example of a branched organ in which co-alignment of the airways and blood vessels encompass all branching generations ranging from the primary bronchi to the alveoli where the intimately associated capillary plexus is crucial for efficient gas exchange between the blood system and the exterior surroundings.

[1]Department of Molecular Biology, Hebrew University-Hadassah Medical School, Jerusalem 91120, Israel. [2]Developmental Biology Program, Saban Research Institute, Children's Hospital Los Angeles, Department of Pediatric Surgery, USC Keck School of Medicine, Los Angeles, CA 90089-9034, USA. [3]Department of Medical Biophysics and Nuclear Medicine, Hadassah Hebrew University Hospital, Jerusalem 91120, Israel.

*Author for correspondence (keshet@cc.huji.ac.il)

Accepted 9 March 2011

A large body of literature has highlighted the essential role of epithelial-mesenchymal cross-talk in controlling branching morphogenesis of the airways (Cardoso and Lu, 2006; Hogan, 1999; Hogan and Yingling, 1998). Furthermore, key positive regulators (e.g. FGF10) and negative regulators (e.g. *Shh* and sprouty2) have been identified [for a recent review, see Maeda et al. (Maeda et al., 2007)]. In both human and mouse lungs, epithelial branching is highly stereotypic. However, the developmental program responsible for generating this reproducible branching pattern is incompletely understood. A recent seminal study has delineated all the branching events taking place during early murine lung development (Metzger et al., 2008), defining three distinct modes of branching: domain branching, planar bifurcation and orthogonal bifurcation. These, in turn, are governed by four mechanistic principles: periodicity generation and domain specification (both implicated in domain branching), a bifurcator controlling bifurcations and a rotator required for bifurcations that are also associated with changes in the plane of bifurcation (orthogonal bifurcation).

Previous studies by ourselves and others using vascular manipulations have suggested that vessels might have an impact on epithelial branching, thus adding vascular endothelial cells as a third player to the epithelial-mesenchymal cross-talk (Akeson et al., 2003; Del Moral et al., 2006; Groenman et al., 2007; van Tuyl et al., 2005; Yamamoto et al., 2007). These studies have shown that ex vivo vascular endothelial growth factor (VEGF) inhibition might result in a reduced number of terminal epithelial branches but a possible role for the vasculature in determining branching stereotypy has not been addressed in any organ, let alone in vivo. To address this proposition, several advents were required: a reference map of stereotyped normal branching events during early stages of lung development; a methodology for in vivo vascular ablation under conditions that enable uncoupling of perfusion-dependent and

perfusion-independent roles; and a methodology for high-resolution, 3D co-visualization of epithelial and vascular networks.

Here, we used different strategies of VEGF-based vascular ablation (and, in turn, its re-gain) in vivo, as well as in organ culture to determine the putative non-perfusion-dependent role of blood vessels in each of the individual branching modes recently defined and characterized by Krasnow and co-workers (Metzger et al., 2008).We show that blood vessels are indispensable for the stereotypic 3D patterning of the lung, specifically for events associated with deviations from simple two-dimensional branching.

MATERIALS AND METHODS

Mice and conditional in vivo manipulations

For a conditional loss of VEGF function in the lung, a doxycycline-regulated bi-transgenic system was used. The system is composed of a lung-specific 'driver' line [SpCrtTA mice, kindly provided by Dr Whitsett (Perl et al., 2002)] and a 'responder' line in which a VEGF decoy receptor composed of an IgG1-Fc tail fused to the extracellular domain of VEGFR1 is doxycline-inducible (Grunewald et al., 2006; May et al., 2008). For induction, doxycycline (Dexon) was administered in the drinking water (200 μg/ml doxycycline, 2% w/v sucrose) at day E6.5 and for 'switching-off' transgene expression it was replaced with fresh drinking water. In some experiments, a VEGFR2-*lacZ* reporter transgene (Shalaby et al., 1995) was also crossed-in to visualize the developing vascular tree.

Ectopic mesenchymal FGF10 expression was achieved via the use of triple transgenic mice composed of Dermo1-Cre (Yu et al., 2003), ROSA26-rtTA (The Jackson Laboratory) and floxed;tet(0)Fgf10 (Clark et al., 2001). Ectopic FGF10 expression was induced at E11.5 by switching to doxycycline-supplemented food (25 mg/g; Harlan Teklad, Madison, WI, USA). Animal care and experiments were approved by the Institutional Animal Care and Use Committee of the Hebrew University.

Lung explants and ex vivo vascular manipulations

Wild-type ICR:Hsd (CD-1) or transgenic SpCrtTA/I-sVEGFR1 embryos were dissected at either E11.5 or E12.5 in cold HBSS (Biological Industries) and embryonic lungs were removed. Lung explants were cultured in 1 ml DMEM F12 medium (Gibco) supplemented with 50 U/ml penicillin/streptomycin (Biological Industries) and 5% fetal bovine serum (Biological Industries) at the air fluid interface upon an 8.0-μm Nuclepore Track-Etch membrane (Whatman). Explants were incubated at 37°C in a humidified 5% CO_2 atmosphere and medium was replaced every 48 hours. For activation of sVEGFR1 transgene, 100 nM doxycyline was added to the medium upon culturing and double-transgene explants were compared with mono-transgene littermates. For pharmacological vascular ablation, a VEGFR2 intracellular inhibitor (termed U7) based on the N-phenyl-N0-[4-(4-quinolyloxy)phenyl] urea skeleton (Kubo et al., 2005) was used at a concentration of 100 nM. U7 was added to the medium upon culturing and either washed out at 48 hours or freshly added with each medium change. For conditioned medium experiments, U7 was washed out at 48 hours and replaced with lung medium (as described above) conditioned for 12 hours with either HUVEC cells or primary human epithelial skin cells. Conditioned medium was centrifuged for 8 minutes at 1200 rpm (2400 ***g***) before being added to the explants.

Immunohistochemistry

For whole-mount immunostaining, E11.5 or E12.5 embryos were dissected in PBS and lungs were fixed for 2 hours in 4% paraformaldehyde at 4°C, washed in PBS and dehydrated gradually in up to 100% methanol. Lung explants were fixed in methanol:DMSO (4:1) for 2 hours at 4°C and transferred to 100% methanol. In vivo samples and explants were then double immunostained using a 3 day protocol. Briefly, samples were blocked by incubation in Cas-Block (Invitrogen) and 0.5% Triton X-100 for 2 (explants) or 4 (in vivo samples) hours followed by overnight incubation with primary antibodies at 4°C. Samples were then either washed or incubated with Biotin-SP-AffiniPure donkey anti-rat IgG (Jackson) for 5 hours at room temperature and finally incubated overnight with secondary antibodies in 1% BSA (Amresco) in PBS at 4°C. For E13.5 and older lungs, a modified, longer protocol was used: fixation and dehydration was similar followed by 24 hours of quenching in methanol:DMSO:H_2O_2 (2:1:3) at room temperature followed by three to five 1-hour incubations at –80°C interspersed with thawing to room temperature. Blocking was carried out by incubating for 24 hours in 10% serum in TBST with 0.01% NaAz at room temperature. Samples were then incubated with primary antibodies for 48 hours at room temperature, washed overnight at room temperature and incubated with secondary antibodies for an additional 48 hours at room temperature.

The following antibodies were used: rat anti-CD31 (1:50, BD Pharmingen), mouse anti-E-Cadherin (1:100, BD Pharmingen), rabbit anti-phosphoHistone-3 (1:100, Cell Signaling), rabbit anti-cleaved caspase 3 (1:100, Cell Signaling). Secondary antibodies were all from Jackson as follows: Biotin-SP-AffiniPure donkey anti-rat IgG (1:200) Cy5-conjugated streptavidin (1:100), Cy3-conjugated donkey anti-mouse (1:100), Cy2-conjugated donkey anti-rabbit (1:100).

For immunostaining of thin (3 μm) sections, 4% paraformaldehyde-fixed paraffin-embedded specimens were used. Briefly, sections were rehydrated and antigen retrieval was performed using a PickCell pressure cooker. The following primary antibodies were used: hypoxyprobe [1:100, Chemicon; in this case, pimonidazole was injected intraperitoneally (60 mg/kg) 30 minutes prior to sacrifice], cleaved caspase-3 (1:100, Cell Signaling), phosphoHistone-3 (1:100, Cell Signaling). TUNEL staining was performed using a Cell Death Detection Kit (Roche).

Confocal scanning and 3D reconstruction

All immunofluorescent specimens were captured on an Olympus FluoView FV1000 Confocal Microscope. *z*-stacking was performed by automated functions scanning at preset optimal intervals depending on the lens in use. 3D reconstructions of *z*-stack scans were performed by Bitplane IMARIS 6.0.1 software. Volume and isosurface functions were used. For supplementary movies, animation functions were used.

Data analysis

Proliferating endothelial cells were visualized by double immunostaining with pH3 and E-Cadherin and were quantified by processing digital images with the aid of ImageJ software calculating the number of double-positive cells per an epithelial surface area unit.

Quantification of in vivo anterior/posterior (A/P) versus dorsal/ventral (D/V) branching was carried out by 360° rotation of 3D reconstructed images of E12.5 lungs and counting the number of branches on each axis. Branching angles were measured by generating digital pictures of transverse 'slices' of the 3D reconstructions. AutoCad 2007 software (by Autodesk) was used to determine the angle between the stem of the branch and the corresponding A/P plane. Quantification of vertical (D/V) versus planar (A/P) branching in lung explants was performed by generating coronal slices of the entire volume of each explant (*z*-stack of the entire volume) and counting the number of symmetrical airway circles (indicating a branch formed on the D/V plane) and terminal branches (indicating a branch formed on the A/P plane). The length of each D/V branch, in vivo and ex vivo, was calculated by multiplying the number of the consecutive confocal slices in which the branch appeared by the *z*-stack interval (1.2-4.7 μm). Statistical analysis was performed using two-tailed Student's *t*-test. Data are presented as mean ± s.d.

Whole-mount in situ hybridization

Lungs were fixed in 4% paraformaldehyde for 20 minutes and whole-mount in situ hybridization was performed based on a previously described protocol (Winnier et al., 1995). Mouse FGF10, Sprouty2 and Shh cDNAs were used as templates for the synthesis of digoxigenin-labeled antisense riboprobes.

Real-time PCR analysis

cDNA was generated from total RNA by using the Reverse-iT 1st Strand Synthesis kit (ABgene) and the respective primers. Relative levels of expression were determined by SYBR green real-time PCR normalized to GAPDH mRNA level of expression.

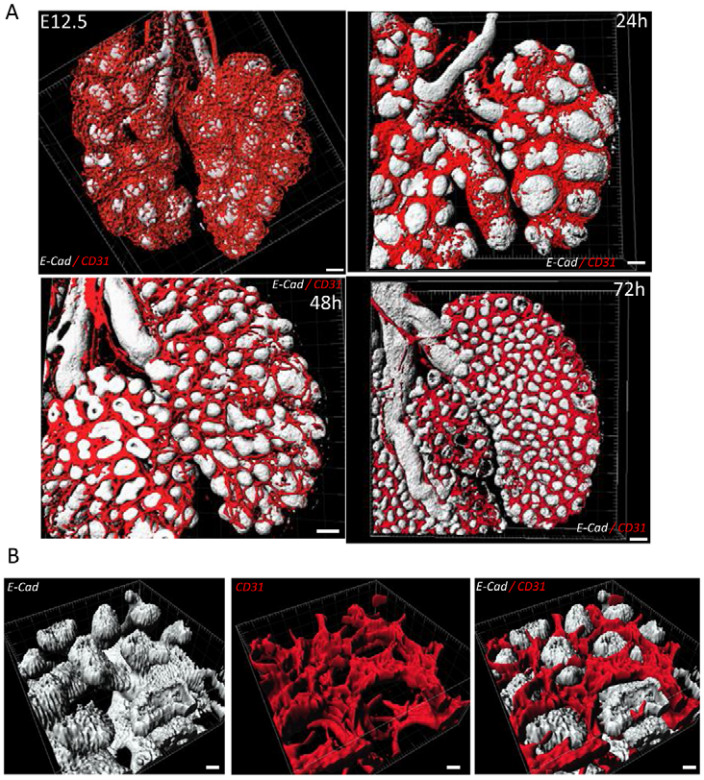

Fig. 1. The basic branching unit of an epithelial bud surrounded by a capillary plexus is preserved during ex vivo ramification. (**A**) Developing mouse lungs were dissected at E12.5 (top left) and grown ex vivo at the air-medium interface for 24, 48 and 72 hours. Double immunostaining of whole mounts for E-cadherin (E-Cad) and CD31 was performed followed by confocal-aided *z*-stacking of images and 3D reconstruction. For reconstruction, E-cad was pseudocolored in white and CD31 in red. Scale bars: 100 μm. (**B**) Higher magnification of a representative lung explant maintained in culture for 72 hours. Scale bars: 20 μm.

X-gal staining

Tissue was fixed with 4% paraformaldehyde in PBS for 15 minutes on ice followed by two washes in rinse solution (PBS containing 2 mM $MgCl_2$, 0.01% sodium deoxycholate and 0.02% Nonidet P-40) prior to addition of 5 mM of ferrocyanide, 5 mM ferricyanide and 1 mg/ml X-gal.

DNA mass quantification

DNA mass in experimentally manipulated lungs was quantified by extracting whole organ DNA (for E12.5 lungs) or left lobe DNA (for postnatal lungs) with a QIAGEN DNeasy tissue kit and measuring DNA content using a NanoDrop ND-1000 Spectrophotometer.

RESULTS

The basic branching unit of an epithelial bud surrounded by a capillary plexus is preserved during ex vivo ramification

Most studies employing lung explants have thus far focused on epithelial-mesenchymal interactions during ex vivo ramification rather than on co-ramification of epithelial and vascular components. Here, we used the endothelial cell marker CD31 and the epithelial-specific marker E-cadherin to visualize both networks during progressive stages of ex vivo ramification. Confocal microscopy in conjunction with high resolution three-dimensional reconstruction of epithelial and vascular trees allowed us to visualize their inter-relationship. Lungs were explanted at E12.5 and maintained in culture for different durations up to 72 hours. As shown in Fig. 1, at the time of resection each epithelial bud was intimately surrounded by a dense capillary plexus resembling the configuration in alveoli. Remarkably, the basic structural unit of an epithelial bud surrounded by a dense capillary plexus was preserved throughout extensive further branching (Fig. 1 and see Movie 1 in the supplementary material). These results indicate that coordinated development of epithelial and endothelial tubes is essentially independent of systemic cues or flow, in general, and of perfusion and nutritional cues, in particular. It thus appears that vascular/endothelial proximity must be governed by intrinsic factors in the respective cell types.

Vascular ablation in vivo using a decoy VEGF receptor

To determine how vascular cells impact epithelial branching, we developed a transgenic system suitable for reducing the vasculature in the developing lung in vivo. The system is based on conditional loss of VEGF function, exploiting the fact that precluding VEGF signaling during early stages of lung development leads to a vascular deficit without adversely affecting the epithelium and mesenchyme. Briefly, a VEGF decoy receptor (sVEGFR1) was conditionally induced via switching ‘on’ expression of a transactivator protein (SP-C; SFPTC – Mouse Genome Informatics) driven by a lung-specific promoter (Fig. 2A). Initial experiments have shown that although the induced decoy receptor is a secreted protein, no phenotype was observed in tissues other than the lung, embryos appeared in the normal Mendelian frequency and there was no difference in gross morphology or size of non-lung organs (see Fig. S1 in the supplementary material). As shown in Fig. 2B and quantified in Fig. 2D, VEGF blockade did indeed lead to a progressive reduction in microvascular density. A markedly reduced vasculature due to VEGF inhibition was also evidenced with the aid of a reporter transgene composed of β-galactosidase knocked-in onto the native *Vegfr2* (*Kdr* – Mouse Genome Informatics) locus (see Fig. S2 in the supplementary material). Prior to analysis of ensuing phenotypes, it was necessary to determine the extent to which vascular loss results in hypoxia and tissue damage in order to rule out phenotypes that are secondary to insufficient perfusion.

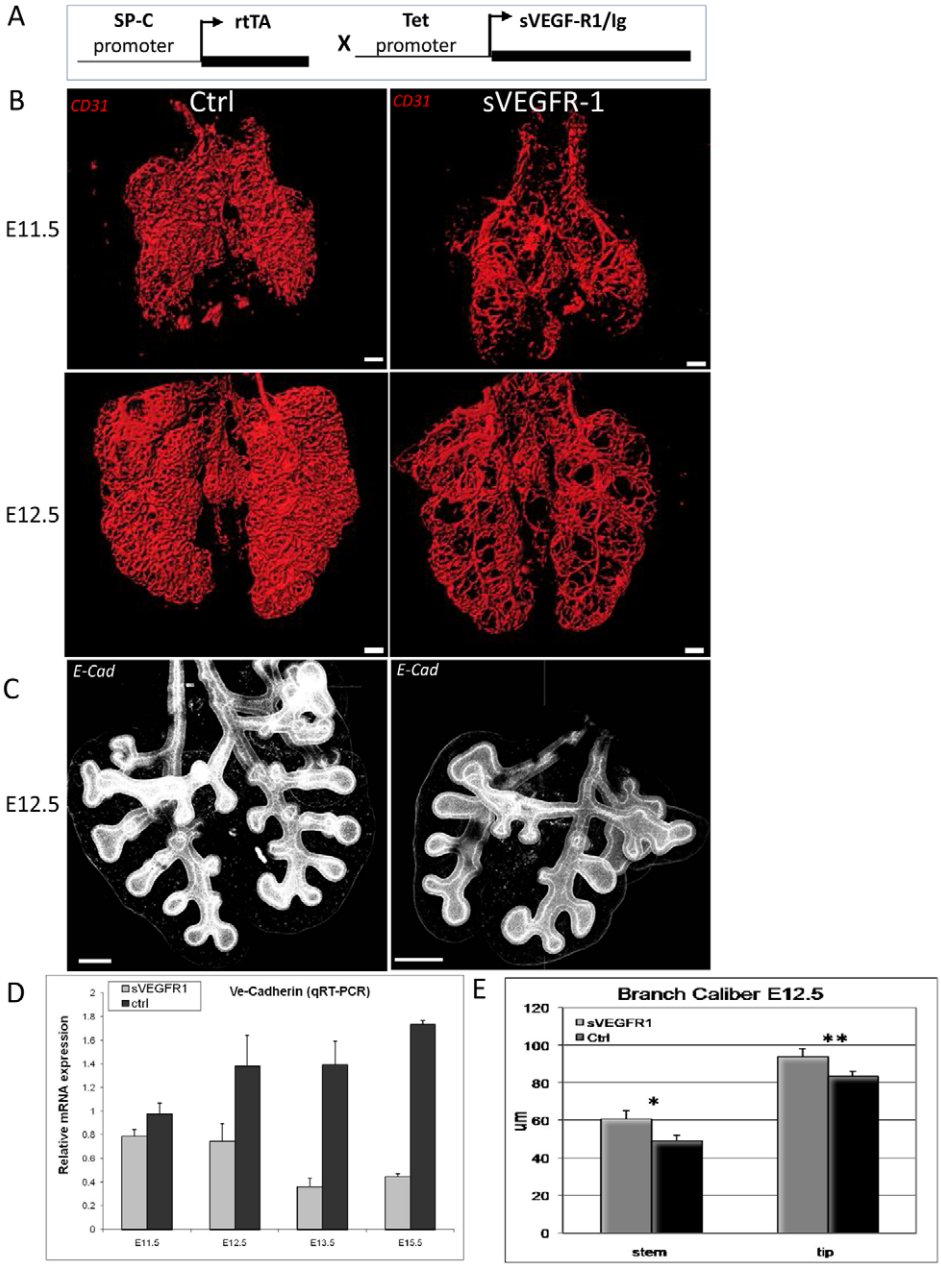

Fig. 2. Vascular reduction in vivo leads to fewer, more dilated airway branches. (**A**) Schematic of the bi-transgenic system employed for a conditional VEGF blockade (see Materials and methods for details). (**B**) sVEGFR1 was induced at E6.5, mouse lungs were dissected on the indicated day and processed for whole-mount immunostaining for CD31. Images depict 3D reconstructions of the entire lung. Scale bars: 100 μm. (**C**) 2D projection of *z*-stack confocal images of whole E12.5 littermate lungs stained for E-cadherin (E-Cad) to highlight the airways. Note that the lung with reduced vascularity has fewer and more dilated airways. Scale bars: 200 μm. (**D**) Quantification of relative vascular densities by qRT-PCR of VE-cadherin comparing mono-transgenic controls and double-transgenic littermates at each indicated time point (n=6 littermates at each time point). (**E**) Quantification of airway caliber. The caliber of each branch was measured at its stem and tip levels. A significant increase in caliber is seen in vessel-ablated lungs [a 124.3% increase in stem (P<0.03) and a 112.5% increase in tip ($P<1.1\times10^{-9}$)]. n=180 branches in the left lobe of 20 different lungs.

It was found that, at E11.5, vascular loss was not accompanied by detectable tissue hypoxia, as measured directly using Hypoxiprobe and indirectly by a surrogate hypoxia-induced marker gene (*Glut1*; *Slc2a1* – Mouse Genome Informatics) (see Fig. S3 in the supplementary material). At E12.5, although a moderate level of hypoxia was evident, all other parameters indicative of tissue integrity remained normal. There was no morphological evidence of tissue damage, nor evidence of cell death, as judged from both TUNEL (not shown) and caspase-3 staining analyses (see Fig. S4 in the supplementary material). Importantly, epithelial cell proliferation at E12.5 proceeded at a normal rate overall (see Fig. S5 in the supplementary material) as well as regionally in both stem and tip domains of extending branches (see Fig. S6 in the supplementary material). Also, only a modest 19% inhibition was observed in total proliferation, which also includes proliferating mesenchymal and vascular cells (see Fig. S7 in the supplementary material). By contrast, at time points later than E12.5, there was clear evidence of tissue damage. We, therefore, decided to restrict phenotypic analysis to the E11.5-12.5 developmental window, reasoning that compromised perfusion is not yet a significant factor at this early time.

Vascular inhibition results in fewer and more dilated airway branches that can be rescued upon re-vascularization

To determine the consequences of vascular ablation in vivo, we used the transgenic system described above. As shown in Fig. 2C, reducing the lung vasculature led to a marked inhibition in the number of epithelial branching events. Branches that did form had a larger caliber than normal branches (Fig. 2E), which is the expected outcome of less branching while maintaining the normal rate of epithelial cell proliferation.

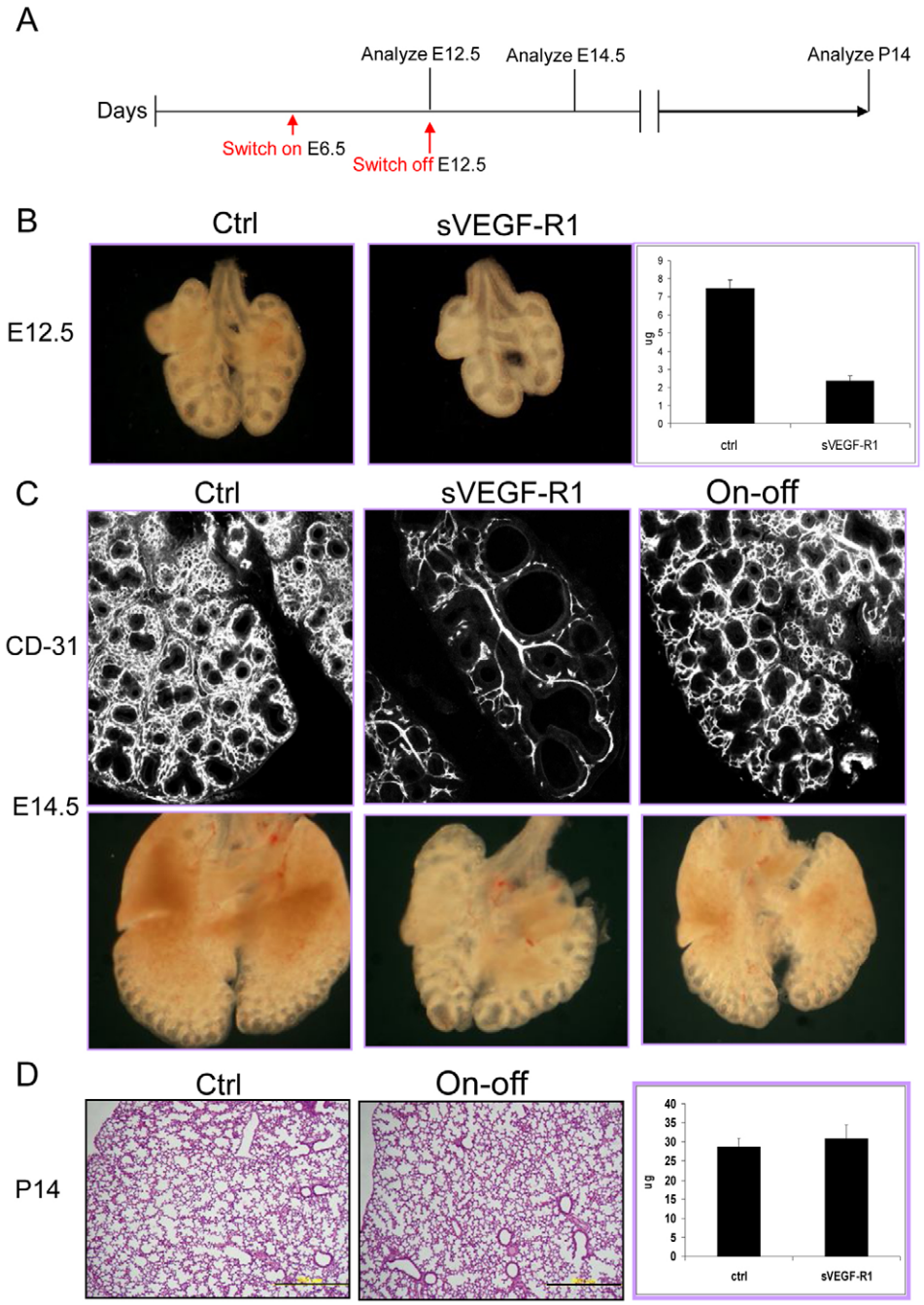

Fig. 3. Reduced branching can be rectified upon re-vascularization. (**A**) Overall experimental design: sVEGFR1 expression was activated at E6.5 and terminated at E12.5 to allow re-vascularization to take place. Lungs were then analyzed at E14.5 and P14 and compared with lungs in which VEGF blockade was maintained until E14.5 (maintaining VEGF blockade for longer than E13.5 results in perinatal death). (**B**) Lungs at E12.5, i.e. at the time of terminating VEGF blockade. Note the markedly reduced size (middle) and lower DNA content (right; *n*=5 control and 5 sVEGFR-1 littermate lungs) associated with reduced vascularity. (**C**) Lungs at E14.5. Note extensive re-vascularization following termination of the VEGF blockade (CD31 staining in top images). Also note partial rescue of lung size and branching arrest (whole-mount views in bottom images). (**D**) P14 lungs. Note complete rescue of lung morphology (Hematoxylin and Eosin stained sections) and a comparable DNA content (right) in control and 'on/off' mice (*n*=5 control and 4 littermate lungs). Scale bars: 500 μm.

To examine whether re-vascularization would rescue branching arrest, we took advantage of the ability to terminate the VEGF blockade at will and resume VEGF-instructed angiogenesis. VEGF blockade was terminated at E12.5 and lungs were retrieved for analysis at E14.5 or P14 and compared with lungs of the corresponding developmental time point subjected to a continuous VEGF blockade, as well as to control littermates (see protocol in Fig. 3A). By E12.5, i.e. at the time of switching off sVEGFR1, lung growth was retarded, manifested in a marked reduction in overall DNA content (Fig. 3B). As expected, removal of VEGF inhibition resulted in resumption of re-vascularization showing a nearly complete vascular re-gain by E14.5 (Fig. 3C). Relative quantification of vascular densities indicated a 4.1-fold higher density ($P<1.4\times10^{-32}$) relative to E14.5 lung continuously maintained in the 'on' mode and was lower than control E14.5 lungs by only 13% ($P<0.0003$). Re-gain of normal vascular density was completed by E18.5 (not shown). Remarkably, vascular re-gain was accompanied by partial rescue of branching arrest at E14.5 (Fig. 3C) and complete rescue at P14, so that lungs were now indistinguishable from control lungs (Fig. 3D). Notably, the markedly reduced size of the lung was also fully rescued by day P14, as evident from both a comparable lung weight (not shown) and its similar overall DNA content (Fig. 3D).

Taken together, these results indicate that the interrupted developmental program can resume even after a significant delay, arguing against totally inflexible developmental 'clocking'. Also, the catching-up of normal organ size highlights the robustness of lung size control mechanisms.

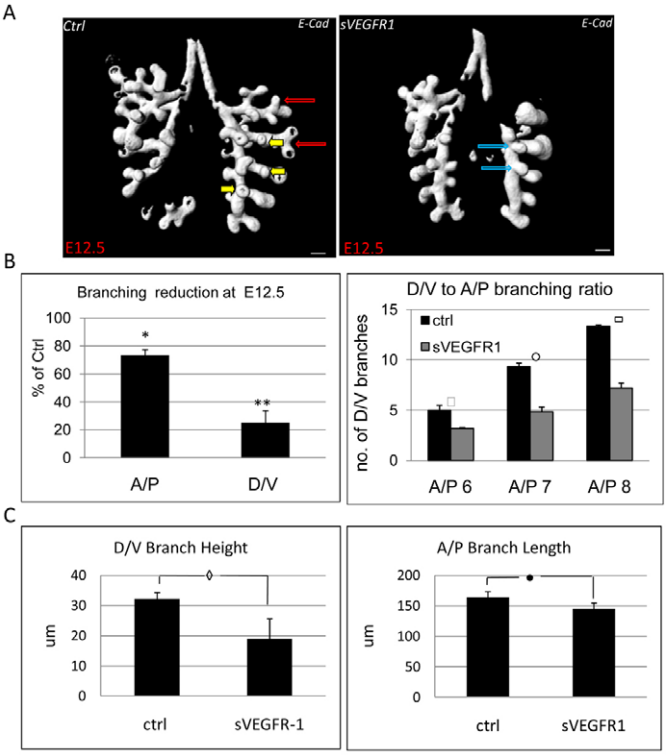

Fig. 4. Domain branching requiring a change in branching plane is preferentially inhibited by in vivo vascular ablation. (**A**) 3D reconstruction (IMARIS software-aided reconstruction) of *z*-stacked confocal images from E12.5 mouse lungs immunostained for E-cadherin. Note significantly fewer branches in sVEGFR1-induced lungs. Arrows on the control lung highlight specific branches missing in the manipulated lungs with red arrows pointing at branches extending in the A/P axis and yellow arrows pointing at perpendicular branches. Blue arrows on manipulated lungs indicate D/V branches that did develop but at a sharp angle. (**B**) Preferential inhibition of D/V branching. Left: Quantification of the number of A/P and D/V branches in E12.5 lungs. Results are expressed as percentage of control (*P<0.0004, **P<0.0005). Right: Number of D/V branches standardized to the number of A/P branches in the range of 6-8 A/P branches of the left lobe (square, P<0.05, open circle, P<0.01, rectangle, P<0.004; n=36 control lungs and n=33 sVEGFR-1 lungs). (**C**) Lengths of D/V and A/P branches in control and sVEGFR1-induced lungs. Note a reduction of 11.7% in the length of A/P branches [solid circle, P<0.00002; n=160 branches of the left lobe (LL) and right caudal lobe (RCdL), 25 lungs] compared with a 41.2% reduction in the length of D/V branches (diamond, $P<4\times10^{-11}$; n=105 branches of the LL and RCdL,18 lungs).

Domain branching requiring a change in branching plane is preferentially inhibited by in vivo vascular ablation

We wished to determine whether the vasculature is equally required for all branching events or, alternatively, selectively required for a particular branching mode. Of the four mechanistic principles defined by Metzger et al. as implicated in airway branching, namely, a periodicity generator, a domain specifier, a bifurcator and a rotator (Metzger et al., 2008), the first and third are planar branching events, whereas the second and fourth generate a new domain or branch that is perpendicular to the previous one (i.e. extending to the D/V axis). Because in vivo ablation of the vasculature without inflicting tissue damage could only be exercised at early stages of lung development when domain branching is the predominant branching mode, our in vivo analysis could only differentiate between events implicating a periodicity generator from a domain specifier. To aid this analysis, serial *z*-stack confocal images were used for 3D reconstruction of control and vessel-deficient E12.5 lungs. As shown in Fig. 4, branching perpendicular to the main plane (i.e. D/V branching) was preferentially inhibited as a result of vascular loss relative to branching in the same plane (i.e. A/P branching), which was only marginally affected (Fig. 4A). Relative to controls, D/V branching in E12.5 lungs was inhibited by 75% whereas A/P branching was reduced by only 27% (Fig. 4B, left). To rule out the possibility that this apparent selectivity merely reflects a global delay of branching caused by vascular loss, the number of D/V branches was also standardized relative to a given number of A/P branches rather than relative to developmental timing. As shown, the number of D/V branches was markedly reduced also when compared with a given number of A/P branches in the range of 6-8 A/P branches (Fig. 4B, right). In addition, D/V branches were significantly reduced in length compared with length reduction of A/P branches (Fig. 4C).

Incomplete rotation of D/V branches following in vivo vascular ablation

The finding that branching at the D/V axis was preferentially inhibited suggested that nearby vessels might be required for proper rotation of branching plane. Therefore, we measured branching angles in those cases in which a new branch extending dorsally or ventrally was formed despite vessel ablation, taking advantage of the high resolution of 3D reconstructed lung images. In contrast to control lungs where D/V branching was always at a 90° angle, rotation in vessel-ablated lungs was incomplete and new branches emerged at a sharp angle of less than 40° on average (Fig. 5).

Vascular ablation leads to ectopic airway branching

Normally, branching is highly stereotyped and ectopic branching occurs at a very low frequency. However, in vessel-ablated lungs the frequency of branches unaccounted for by the branching program elucidated by Metzger et al. (Metzger et al., 2008) was markedly increased. Representative pair-wise comparisons of lungs from two different litters are displayed in Fig. 6, showing a mild and a more severe phenotype of ectopic branching. Overall frequency of ectopic branching was increased more than tenfold in vessel-ablated lungs (Fig. 6).

Together, abnormal branching events, encompassing missing, tilted and ectopic branches, tended to take place in areas devoid of vessels more than in areas where vessel ablation was relatively ineffective (see Fig. S8 and Movie 2A,B in the supplementary material).

Considering the fact that each branch serves as a template for all further branching, the defects described above are bound to culminate in a progressively flattened lung structure. It is noteworthy that incomplete rotation and ectopic branching cannot be explained simply by hypoxic stress resulting in a developmental arrest or delay. These results thus highlight an essential role of the vasculature in lung stereospecific patterning and in creating the three-dimensional organ architecture.

Orthogonal bifurcations but not planar bifurcations are inhibited in the absence of vessels: ex vivo analysis

To examine later stages of branching morphogenesis (>E12.5) we turned to an ex vivo explant system, which does not rely on blood vessels for its perfusion. Lungs were cultured at E11.5 and

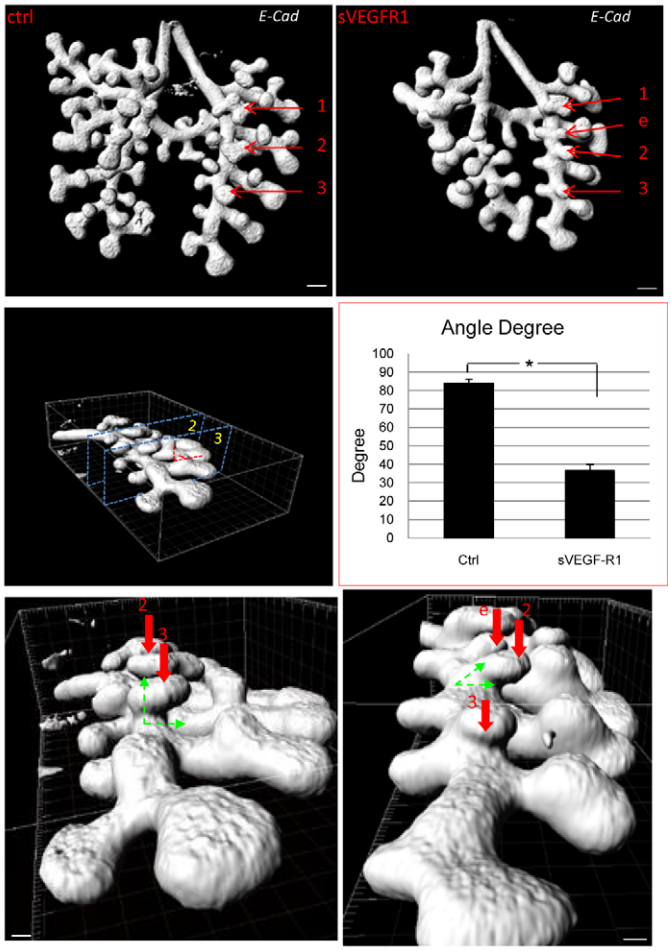

Fig. 5. Incomplete rotation of D/V branches following in vivo vascular ablation. 3D reconstruction of E12.5 mouse lungs obtained as described in Fig. 4 and further analyzed with respect to branching angles. Top panel shows a ventral view of control and manipulated lungs with arrows pointing at three particular branches extending at the D/V axis. Note an ectopic branch (e) in the manipulated lung. To better visualize branching angles, representative 3D reconstructions (bottom images) were tilted as illustrated in the middle left image. Note that the branching angle (the angle between the branch stem and the main plane, green arrows) is significantly reduced in the VEGFR1-induced lung, as also quantified in the histogram (*P<7.8×10^{-12}). Scale bars: top row, 100 μm; bottom row, 50 μm.

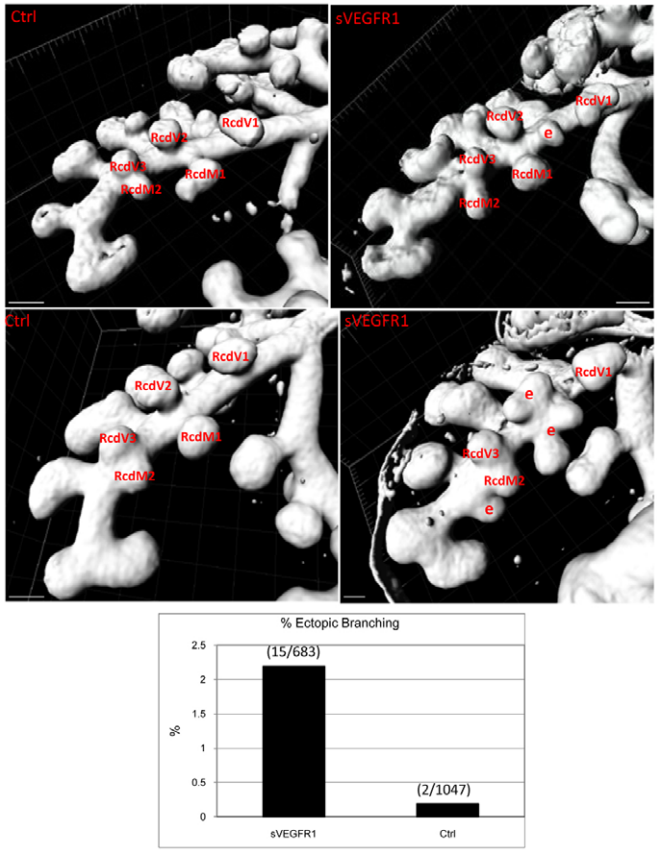

Fig. 6. Vascular ablation leads to ectopic airway branching. Representative 3D reconstructions of control and vessel-ablated littermate E12.5 RCd lobes. Each branch was assigned and named according to its position relative to the detailed branching atlas of Metzger et al. (Metzger et al., 2008). Branches unaccounted for are considered to be ectopic branches (e). The frequency of ectopic branches was increased 11.5-fold in vessel-ablated lungs relative to age-matched control lungs (n=50 control lungs and 34 sVEGFR1 lungs). Right caudal (RCd) lobe, medial (M) 1, 2 and ventral (V) 1-3. Scale bars: 100 μm.

sVEGFR1 was concomitantly activated by addition of doxycyclin to the culture medium (mono-transgenic littermates served as controls). CD31 immunostaining confirmed that VEGF blockade did indeed result in reduced vascular density. However, vascular ablation under this experimental protocol was incomplete and both vessel-poor areas and vessel-rich areas were evident (see Fig. S9 in the supplementary material). This has provided us with a unique opportunity to compare directly the impact of nearby vessels on branching in adjacent regions of the same lung. Remarkably, abnormal branching was confined to regions devoid of blood vessels, as evidenced by much reduced branching and the appearance of abnormally dilated airways specifically in the vessel-free regions (see Fig. S9 in the supplementary material).

Because only partial vascular ablation could be achieved using the genetic approach, we resorted to ex vivo vascular ablation by pharmacological means. To this end, we used a recently described VEGFR2 intracellular inhibitor named U7 (Kubo et al., 2005). Addition of U7 to the explant growth medium resulted in vascular ablation in a dose-dependent manner. At a concentration of 100 nM complete ablation of the vasculature was obtained within 24 hours (see Fig. S10A in the supplementary material). Importantly, endothelial cell apoptosis was not accompanied by any detectable damage to the epithelium and mesenchyme, as judged from histological inspection (see Fig. S10A in the supplementary material). Also, there was no indication for apoptosis of non-endothelial cells beyond that which normally takes place in cultured lung explants (see Fig. S10C in the supplementary material) and, importantly, the normally high rate of epithelial cell proliferation was fully maintained in the presence of U7 (see Fig. S10B in the supplementary material). To ensure that this experimental manipulation did not cause explant collapse, which might have resulted in reduced accessibility of medium components,

measurements of the *z*-axis dimension of 3D reconstructions of entire lung explants were performed. There was no evidence of tissue compression in the vessel-ablated lung (see Fig. S11 in the supplementary material).

The opportunity to maintain explants in culture for at least 72 hours after vessel ablation had been completed, together with continuous branching (see below), enabled us to evaluate directly the impact of vessels on airway branching and patterning in a perfusion-independent setting. From E13.5 and onwards, domain branching was shown to be mostly replaced by a bifurcation mode of both planar and orthogonal configurations. Furthermore, there is a spatial demarcation between planar bifurcation, taking place mostly at the lung periphery and generating terminal buds, and orthogonal bifurcations, taking place more centrally and generating the bulk of the three-dimensional organ (Metzger et al., 2008) (see schematic in Fig. 7C). As shown in Fig. 7, branching proceeded even in the complete absence of vessels and terminal buds were added at a rate comparable to control lungs. This result indicates that branching per se is independent of blood vessels, as was indeed anticipated from numerous previous studies highlighting an epithelial-mesenchymal cross-talk as the underlying mechanism of branching (Hogan and Yingling, 1998; Maeda et al., 2007). However, patterning of newly added branches was affected dramatically by vascular loss. Specifically, whereas the number of planar bifurcation events was reduced by 30%, orthogonal bifurcations were inhibited by 70% (Fig. 7 and see Movie 3A,B in the supplementary material). Moreover, the residual orthogonal bifurcations yielded significantly shorter (56% of control) branches (data not shown).

Thus, the common denominator in phenotypes resulting from in vivo and ex vivo vascular loss appears to be a failure of proper rotation and extension, culminating in overall flat lung morphology.

Vascular loss per se, and not VEGF inhibition, is responsible for branching defects

Given that all procedures used above to ablate the vasculature were based on VEGF inhibition, it remained to be determined whether observed phenotypes are due to VEGF inhibition or due primarily to absence of nearby vessels. Compatible with the latter possibility is our previous observation that exogenous VEGF has no effect on isolated lung epithelium (Del Moral et al., 2006). To discriminate between a direct VEGF effect and a requirement for the physical presence of vessels, U7 was either maintained in the explant culture medium after vessels had been eliminated, or was washed out to relieve VEGF inhibition (thereby also relieving inhibition of other signaling systems that might be inhibited by U7). As evident from Fig. 7C, both treatments yielded an identical phenotype, indicating that endogenous VEGF, which was unable to restore lost blood vessels under these conditions, was also unable to rescue the epithelial branching defects. Furthermore, these defects were not rectified even after exogenous addition of VEGF (data not shown).

As a first step to determine whether the impact of blood vessels on epithelial branching is mediated by endothelial-derived secreted factors, a lung-growth medium conditioned by HUVEC cells was added to vessel-ablated explants. As shown in Fig. S12 in the supplementary material, endothelial conditioned medium could partially rescue the branching defect. A medium conditioned by human primary epithelial cells was unable to rescue the branching defect. Although these results suggest that endothelial-epithelial cell contact might not be required, establishing endothelial specificity in these experiments requires further work.

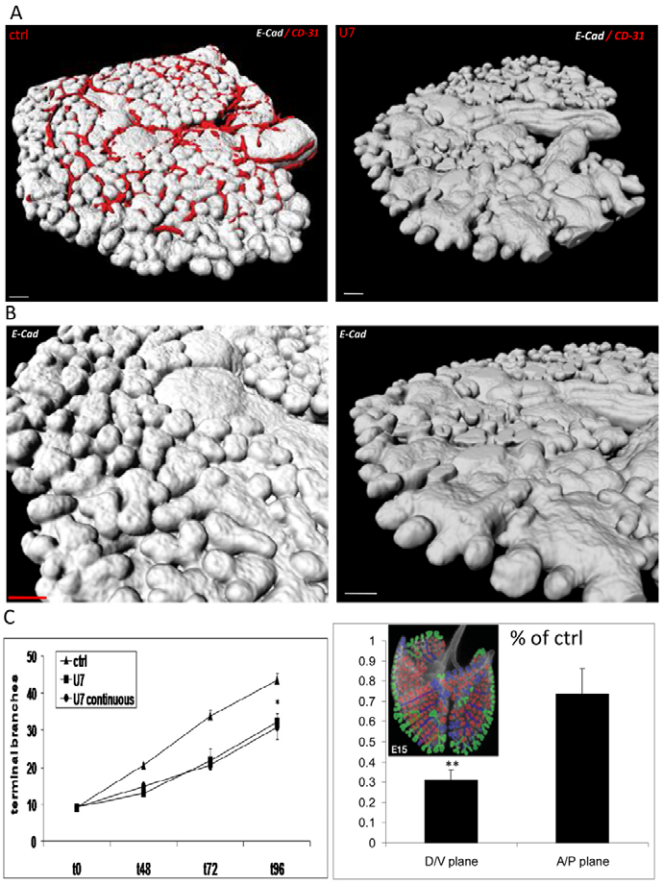

Fig. 7. Vessels are required for orthogonal bifurcations but dispensable for generation of terminal buds by planar bifurcations. (**A**) 3D reconstructions of mouse lungs explanted at E11.5 and maintained in culture for 96 hours. Immunostaining with CD31 (red) confirmed complete vascular ablation by U7. Staining with E-cadherin (E-Cad; white) shows that formation of peripheral branches was significantly less inhibited than central branching. Scale bars: 100 μm. (**B**) High magnification views of the network of epithelial tubes showing vertical projections of new branches in control lung cultures (left) and impaired vertical extension in U7-treated lung cultures (right). Scale bars: 50 μm (red) and 100 μm (white). (**C**) Quantification of the number of terminal buds added in the presence or absence of U7 (left). Note that from t48 onwards, terminal buds are added at a comparable rate (as seen by the graph incline slope=0.4, *n*=106 explants) regardless of whether U7 was washed out at t48 or present throughout the experiment (**P*<0.007 between control and U7 or U7 continuous). Histogram presents *z*-stacking-aided quantification of vertical (D/V) versus planar (A/P) branching, which was performed as described in Materials and methods (***P*<0.002, *n*=8). Note that the area where branches are mostly inhibited corresponds to the area where branching is known to proceed via orthogonal bifurcations. Inset: Reproduced from Metzger et al. (Metzger et al., 2008) with permission, where orthogonal bifurcation are color-coded in red and planar bifurcations in green.

Spatial distribution of key molecular mediators of branching is perturbed in the absence of blood vessels

Previous studies have identified positive and negative regulators of airway branching, highlighting their spatially restricted patterns of expression, most importantly of mesenchymal FGF10 (Bellusci et al., 1997). To determine whether blood vessels might play a role in

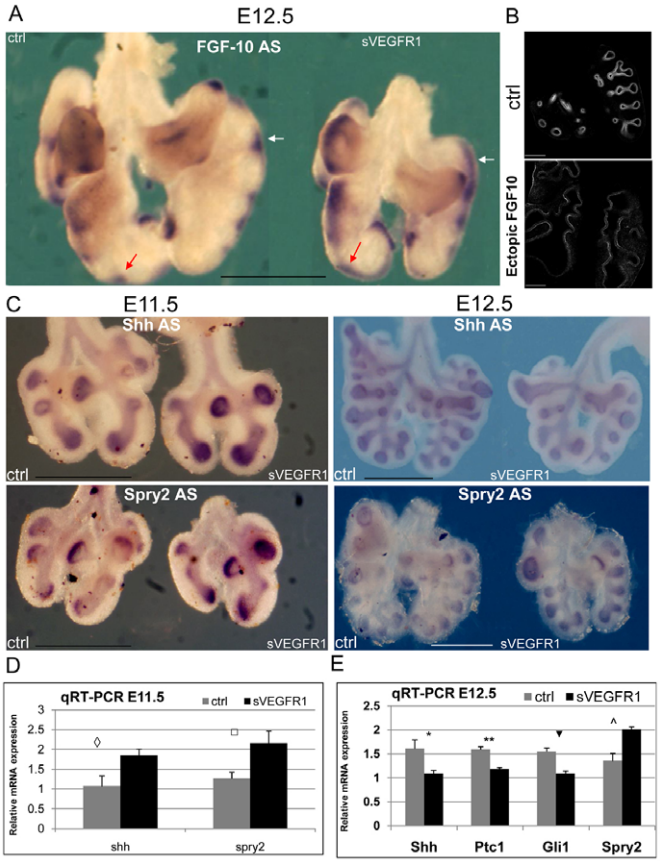

Fig. 8. Vascular loss leads to perturbation in the pattern of FGF10 expression and de-regulated expression of negative regulators of branching. (**A**) FGF10 whole-mount in situ hybridization of littermate control and sVEGFR1-induced E12.5 mouse lungs. Note that instead of punctuated FGF10 expression (highlighted by arrows), vascular loss leads to a more widespread mesenchymal expression. Scale bar: 500 μm. (**B**) Ectopic expression of FGF10 in the mesenchyme was induced at E11.5 as described in Materials and methods and lungs were retrieved at E12.5 and stained with E-cadherin. Note formation of a severe branching arrest and emergence of highly dilated epithelial tubes resulting from ectopic FGF10 expression. Scale bars: 200 μm. (**C**) Whole-mount in situ hybridization of E11.5 and E12.5 lungs for *Shh* and *Spry2*. Note unchanged pattern of expression. Scale bars: 500 μm. (**D**) Quantification by real-time PCR of *Shh* and *Spry2* relative mRNA levels at E11.5 (diamond, $P<0.05$, square, $P<0.01$). (**E**) A similar analysis at E12.5, showing downregulated expression of *Shh* and its downstream targets *Ptc1* and *Gli1* (*$P<0.01$; **$P<0.008$; triangle, $P<0.002$; ^$P<0.02$).

maintaining this unique spatial expression pattern, we performed whole-mount in situ hybridization of control and in vivo vessel-ablated lungs with a FGF10-specific probe at the relevant stages of E11.5 and E12.5. Whereas at E11.5 there was no apparent difference in the spatial distribution of FGF10 between control and manipulated lungs (not shown), at E12.5, the normal punctuated pattern of mesenchymal FGF10 expression, normally evident as focal points juxtapositioned to branching tip, was perturbed in the absence of vessels and was now evident as widespread, poorly focused expression throughout the mesenchyme (Fig. 8A). This result suggests that nearby vessels act to spatially restrict FGF10 expression. The notion that the resultant widespread FGF10 expression in the mesenchyme might lead to abnormal branching was supported by the finding that ectopic expression of FGF10 in the mesenchyme resulted in an abnormal branching phenotype grossly resembling the phenotype caused by vascular loss (Fig. 8B).

Epithelial branching is known to be negatively regulated by sonic hedgehog (SHH), as well as by sprouty2 (Cardoso and Lu, 2006; Warburton et al., 2005). Because vascular loss results in less branching, we reasoned that this might be, at least partially, accounted for by altered spatial distribution and/or expression levels of these negative regulators. Whole-mount in situ hybridization with *Shh*- and sprouty2 (*Spry2* – Mouse Genome Informatics)-specific probes showed that their spatial distribution was unaffected at both E11.5 and E12.5 (Fig. 8C). qRT-PCR analysis revealed that at E11.5 vascular loss was accompanied by upregulated expression of *Shh* and sprouty2 (Fig. 8D). By E12.5, only sprouty2 expression remained abnormally high whereas expression of *Shh*, and its downstream targets *Ptc1* (*Ptch1* – Mouse Genome Informatics) and *Gli1* were expressed at lower levels than control (Fig. 8E), as was expected from previous findings showing that diffused FGF10 pattern is associated with reduced SHH expression (Pepicelli et al., 1998). It remains to be determined whether de-regulated expression of SHH and sprouty2 in the absence of vessels does indeed contribute to abnormal branching. Also, although altered spatial expression patterns of the branching mediators examined here might explain a general inhibition of branching, it comes short of providing a mechanistic explanation for selective inhibition of D/V branching.

DISCUSSION

In this study we used complementary in vivo and ex vivo experimental strategies of vascular manipulations in the developing lung to uncover a novel perfusion-independent role of the vasculature in patterning airway branching. Although previous studies have already ascribed perfusion-independent roles for endothelial cells in determining cell fate commitment in the liver and pancreas, our study is the first to ascribe a role for the vasculature in determining the organ three-dimensional architecture at a later stage of development. This, we find, is brought about by controlling directionality of airway branching and, specifically, of perpendicular rotation from the preceding branching plane.

Previous studies on branching morphogenesis, mostly focusing on epithelial-mesenchymal cross-talk, have provided mechanistic insights on branching at the level of the individual branching event but very little is known regarding the stereospecificity of branching at the whole organ level. Our study, we believe, represents a key first step in this direction by highlighting the indispensable role of the vasculature in 3D patterning of airway branching. We show that blood vessels are less crucial for the branching process per se, as addition of new terminal branches proceeded at a nearly normal rate following vascular ablation. However, blood vessels appear to be essential for maintaining normal branching directionality. Because each newly formed branch serves as a template for further branching, periodic changes in branching planes are essential for making a complex three-dimensional organ rather than a ‘flat’ organ structure. In the lung, in particular, this is crucial for the formation of sufficient gas exchange surfaces within a limited space. Indeed, vascular loss is shown here to result in overall ‘flat’ lung morphology. A requirement of nearby vessels for a change in branching plane is evidenced by the complete absence of most vertical sprouts and incomplete rotation and reduced length of those vertical sprouts that do form in the absence of vessels. This is observed for both rotations associated with domain branching, as well as for rotations taking place during orthogonal bifurcation.

The notion that vessels are essential for three-dimensional branching was further supported by reversal experiments demonstrating that lungs in which the normal branching pattern was perturbed were capable of restoring normal branching when vessels were re-gained even after a few days of delay. Notably, the reduced size of the avascular lung could also be rescued by re-vascularization and its mass after birth was indistinguishable from that of control, indicative of a robust organ size control in the lung. For comparison, studies examining the ability of other under-sized developing organs to re-gain to their normal size showed that this is possible in the liver but not in the pancreas (Stanger et al., 2007).

Open key questions concern the mechanism(s) by which blood vessels might control branching patterns. Importantly, this study clearly rules out mediatory roles of systemic cues or flow, as selective inhibition of vertical sprouting was also observed ex vivo. The finding that ex vivo, i.e. without a systemic connection, blood vessels continued to ramify alongside epithelial tubes, preserving the basic in vivo structure, is compatible with a paracrine affect of the endothelium. In principle, this might be mediated either by secreted endothelially produced factors or, alternatively, by endothelial-epithelial cell contacts. Supporting the former is our preliminary finding that medium conditioned by endothelial cells can partially rectify the branching impediment caused by vascular ablation ex vivo (see Fig. S12 in the supplementary material). Consistent with the later, is our in vivo observation of discrete spiraling points of contact (‘kissing points’) between the endothelium and developing epithelial tubes (see Fig. S13 in the supplementary material).

There are two types of branching defects caused by vascular ablation: first, an overall reduction in branching events while maintaining a normal rate of epithelial proliferation; second, perturbation of sprouting directionality. It is possible that these two phenotypes are mechanistically different. A plausible explanation for the first is a requirement for nearby vessels in order to restrict focally FGF10 expression yielding its typical stereotypic pattern known to dictate branching points. Consistent with this interpretation are the observations that a ‘smeary’ FGF10 expression is correlated with generating ectopic branches at both A/P and D/V axes. The mechanism underlying the second phenotype is at present obscure. The study of Metzger et al. (Metzger et al., 2008) defined the basic patterning and morphogenesis operations repeatedly used during airway branching. Among these, the key to creation of a three-dimensional structure is re-orientation of the new domain or bifurcation plane by 90° between events. It appears that this basic operation is defective in the absence of vessels. Although the molecular identity of the mediator factor(s) is unknown, our results suggest that it is produced or affected by the endothelium. The experimental systems developed here might be harnessed as a platform to elucidate molecular mediators of the vascular-epithelial cross-talk.

Acknowledgements

This study was supported by research grants from the NIH (RO1 HL075773 to D.W. and E.K.) and by the Israel Science Foundation (to E.K.). Deposited in PMC for release after 12 months.

Competing interests statement

The authors declare no competing financial interests.

Supplementary material

Supplementary material for this article is available at http://dev.biologists.org/lookup/suppl/doi:10.1242/dev.060723/-/DC1

References

Akeson, A. L., Greenberg, J. M., Cameron, J. E., Thompson, F. Y., Brooks, S. K., Wiginton, D. and Whitsett, J. A. (2003). Temporal and spatial regulation of VEGF-A controls vascular patterning in the embryonic lung. *Dev. Biol.* **264**, 443-455.

Bellusci, S., Grindley, J., Emoto, H., Itoh, N. and Hogan, B. L. (1997). Fibroblast growth factor 10 (FGF10) and branching morphogenesis in the embryonic mouse lung. *Development* **124**, 4867-4878.

Cardoso, W. V. and Lu, J. (2006). Regulation of early lung morphogenesis: questions, facts and controversies. *Development* **133**, 1611-1624.

Clark, J. C., Tichelaar, J. W., Wert, S. E., Itoh, N., Perl, A. K., Stahlman, M. T. and Whitsett, J. A. (2001). FGF-10 disrupts lung morphogenesis and causes pulmonary adenomas in vivo. *Am. J. Physiol. Lung Cell. Mol. Physiol.* **280**, L705-L715.

Cleaver, O. and Melton, D. A. (2003). Endothelial signaling during development. *Nat. Med.* **9**, 661-668.

Del Moral, P. M., Sala, F. G., Tefft, D., Shi, W., Keshet, E., Bellusci, S. and Warburton, D. (2006). VEGF-A signaling through Flk-1 is a critical facilitator of early embryonic lung epithelial to endothelial crosstalk and branching morphogenesis. *Dev. Biol.* **290**, 177-188.

Groenman, F. A., Rutter, M., Wang, J., Caniggia, I., Tibboel, D. and Post, M. (2007). Effect of chemical stabilizers of hypoxia-inducible factors on early lung development. *Am. J. Physiol. Lung Cell. Mol. Physiol.* **293**, L557-L567.

Grunewald, M., Avraham, I., Dor, Y., Bachar-Lustig, E., Itin, A., Jung, S., Chimenti, S., Landsman, L., Abramovitch, R. and Keshet, E. (2006). VEGF-induced adult neovascularization: recruitment, retention, and role of accessory cells. *Cell* **124**, 175-189.

Hogan, B. L. (1999). Morphogenesis. *Cell* **96**, 225-233.

Hogan, B. L. and Yingling, J. M. (1998). Epithelial/mesenchymal interactions and branching morphogenesis of the lung. *Curr. Opin. Genet. Dev.* **8**, 481-486.

Kubo, K., Shimizu, T., Ohyama, S., Murooka, H., Iwai, A., Nakamura, K., Hasegawa, K., Kobayashi, Y., Takahashi, N., Takahashi, K. et al. (2005). Novel potent orally active selective VEGFR-2 tyrosine kinase inhibitors: synthesis, structure-activity relationships, and antitumor activities of N-phenyl-N′-{4-(4-quinolyloxy)phenyl}ureas. *J. Med. Chem.* **48**, 1359-1366.

Lammert, E., Cleaver, O. and Melton, D. (2001). Induction of pancreatic differentiation by signals from blood vessels. *Science* **294**, 564-567.

Lu, P. and Werb, Z. (2008). Patterning mechanisms of branched organs. *Science* **322**, 1506-1509.

Maeda, Y., Dave, V. and Whitsett, J. A. (2007). Transcriptional control of lung morphogenesis. *Physiol. Rev.* **87**, 219-244.

Matsumoto, K., Yoshitomi, H., Rossant, J. and Zaret, K. S. (2001). Liver organogenesis promoted by endothelial cells prior to vascular function. *Science* **294**, 559-563.

May, D., Gilon, D., Djonov, V., Itin, A., Lazarus, A., Gordon, O., Rosenberger, C. and Keshet, E. (2008). Transgenic system for conditional induction and rescue of chronic myocardial hibernation provides insights into genomic programs of hibernation. *Proc. Natl. Acad. Sci. USA* **105**, 282-287.

Metzger, R. J., Klein, O. D., Martin, G. R. and Krasnow, M. A. (2008). The branching programme of mouse lung development. *Nature* **453**, 745-750.

Pepicelli, C. V., Lewis, P. M. and McMahon, A. P. (1998). Sonic hedgehog regulates branching morphogenesis in the mammalian lung. *Curr. Biol.* **8**, 1083-1086.

Perl, A. K., Tichelaar, J. W. and Whitsett, J. A. (2002). Conditional gene expression in the respiratory epithelium of the mouse. *Transgenic Res.* **11**, 21-29.

Shalaby, F., Rossant, J., Yamaguchi, T. P., Gertsenstein, M., Wu, X. F., Breitman, M. L. and Schuh, A. C. (1995). Failure of blood-island formation and vasculogenesis in Flk-1-deficient mice. *Nature* **376**, 62-66.

Stanger, B. Z., Tanaka, A. J. and Melton, D. A. (2007). Organ size is limited by the number of embryonic progenitor cells in the pancreas but not the liver. *Nature* **445**, 886-891.

van Tuyl, M., Liu, J., Wang, J., Kuliszewski, M., Tibboel, D. and Post, M. (2005). Role of oxygen and vascular development in epithelial branching morphogenesis of the developing mouse lung. *Am. J. Physiol. Lung Cell. Mol. Physiol.* **288**, L167-L178.

Warburton, D., Bellusci, S., De Langhe, S., Del Moral, P. M., Fleury, V., Mailleux, A., Tefft, D., Unbekandt, M., Wang, K. and Shi, W. (2005). Molecular mechanisms of early lung specification and branching morphogenesis. *Pediatr. Res.* **57**, 26R-37R.

Winnier, G., Blessing, M., Labosky, P. A. and Hogan, B. L. (1995). Bone morphogenetic protein-4 is required for mesoderm formation and patterning in the mouse. *Genes Dev.* **9**, 2105-2116.

Yamamoto, H., Yun, E. J., Gerber, H. P., Ferrara, N., Whitsett, J. A. and Vu, T. H. (2007). Epithelial-vascular cross talk mediated by VEGF-A and HGF signaling directs primary septae formation during distal lung morphogenesis. *Dev. Biol.* **308**, 44-53.

Yu, K., Xu, J., Liu, Z., Sosic, D., Shao, J., Olson, E. N., Towler, D. A. and Ornitz, D. M. (2003). Conditional inactivation of FGF receptor 2 reveals an essential role for FGF signaling in the regulation of osteoblast function and bone growth. *Development* **130**, 3063-3074.

A

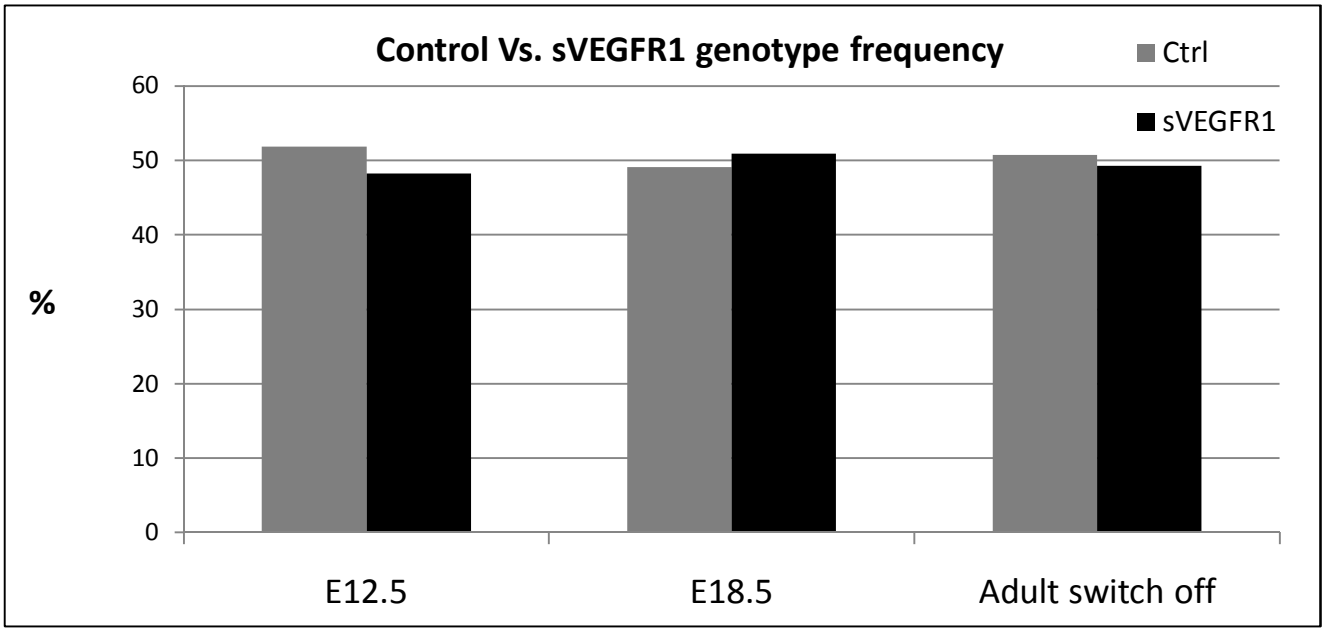
Control Vs. sVEGFR1 genotype frequency
Ctrl
sVEGFR1
%
60
50
40
30
20
10
0
E12.5
E18.5
Adult switch off

B

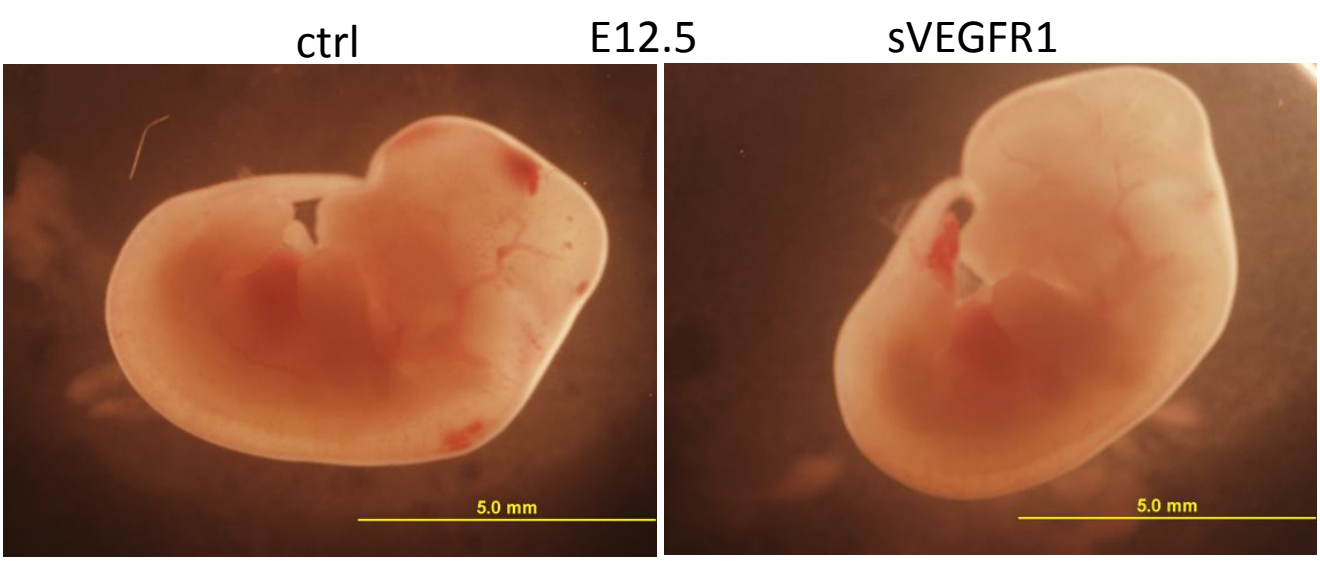
ctrl
E12.5
sVEGFR1
5.0 mm
5.0 mm

C

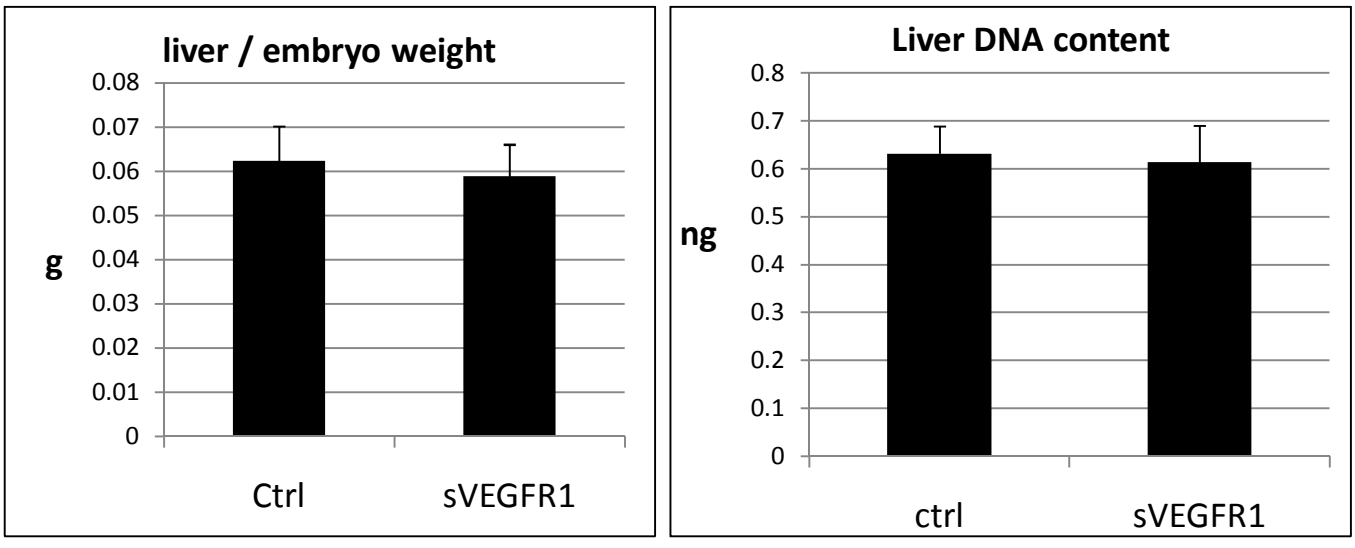
E12.5
liver / embryo weight
g
0.08
0.07
0.06
0.05
0.04
0.03
0.02
0.01
0
Ctrl
sVEGFR1
Liver DNA content
ng
0.8
0.7
0.6
0.5
0.4
0.3
0.2
0.1
0
ctrl
sVEGFR1

E12.5

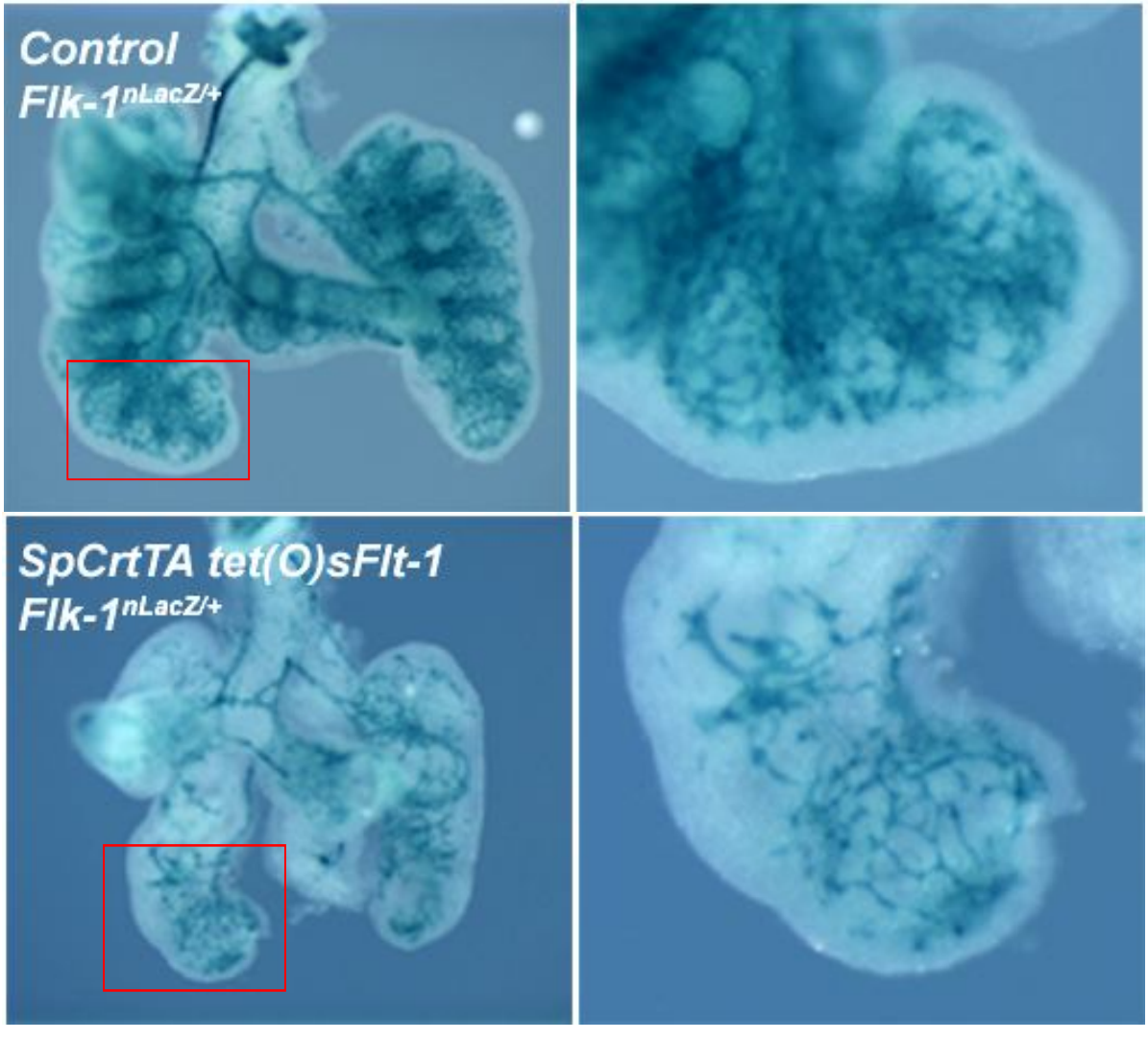

A

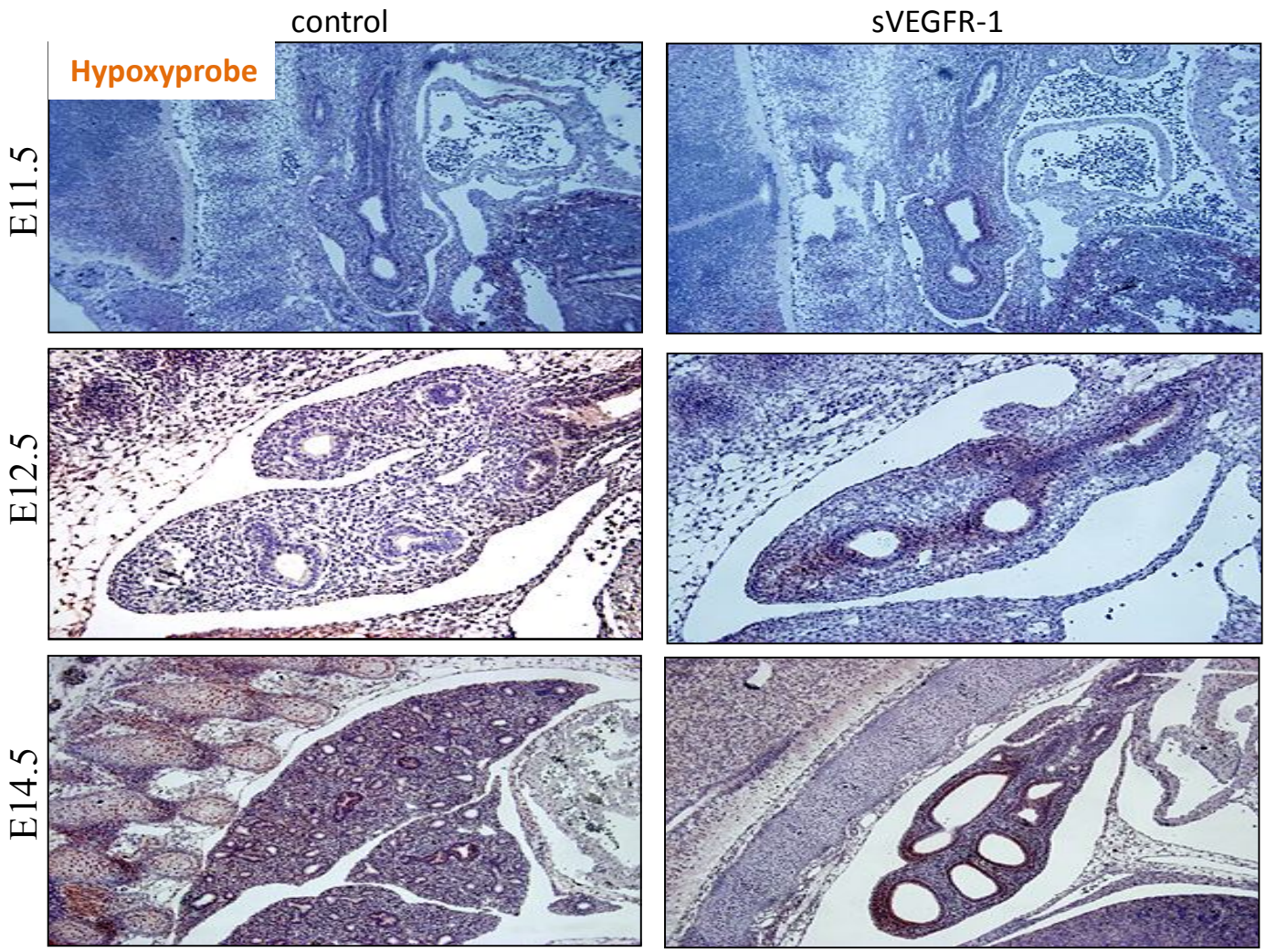
control
sVEGFR-1
Hypoxyprobe
E11.5
E12.5
E14.5

B

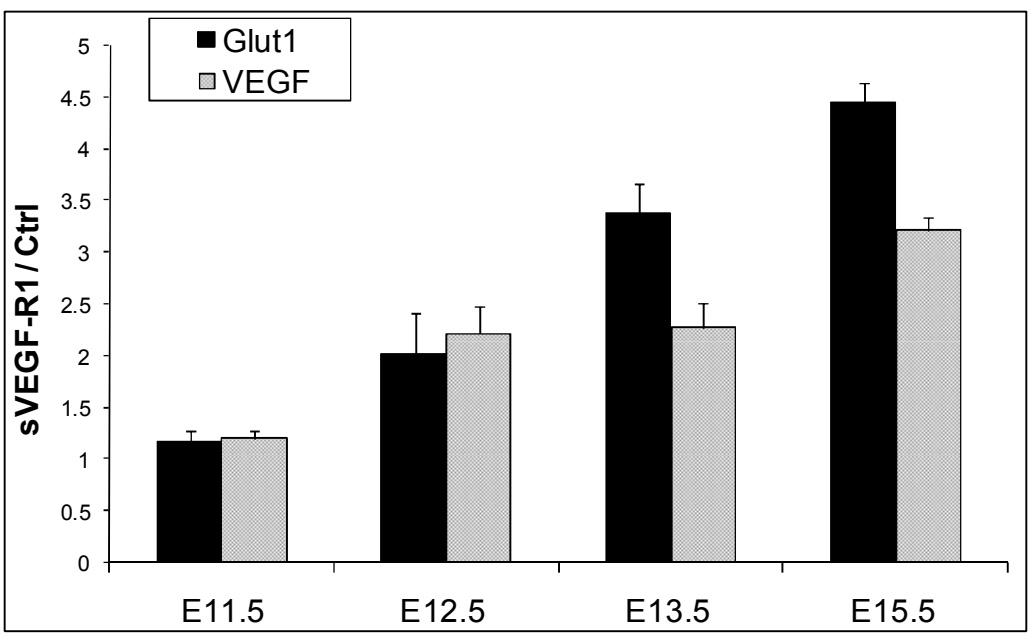
Glut1
VEGF
sVEGF-R1 / Ctrl
5
4.5
4
3.5
3
2.5
2
1.5
1
0.5
0
E11.5
E12.5
E13.5
E15.5

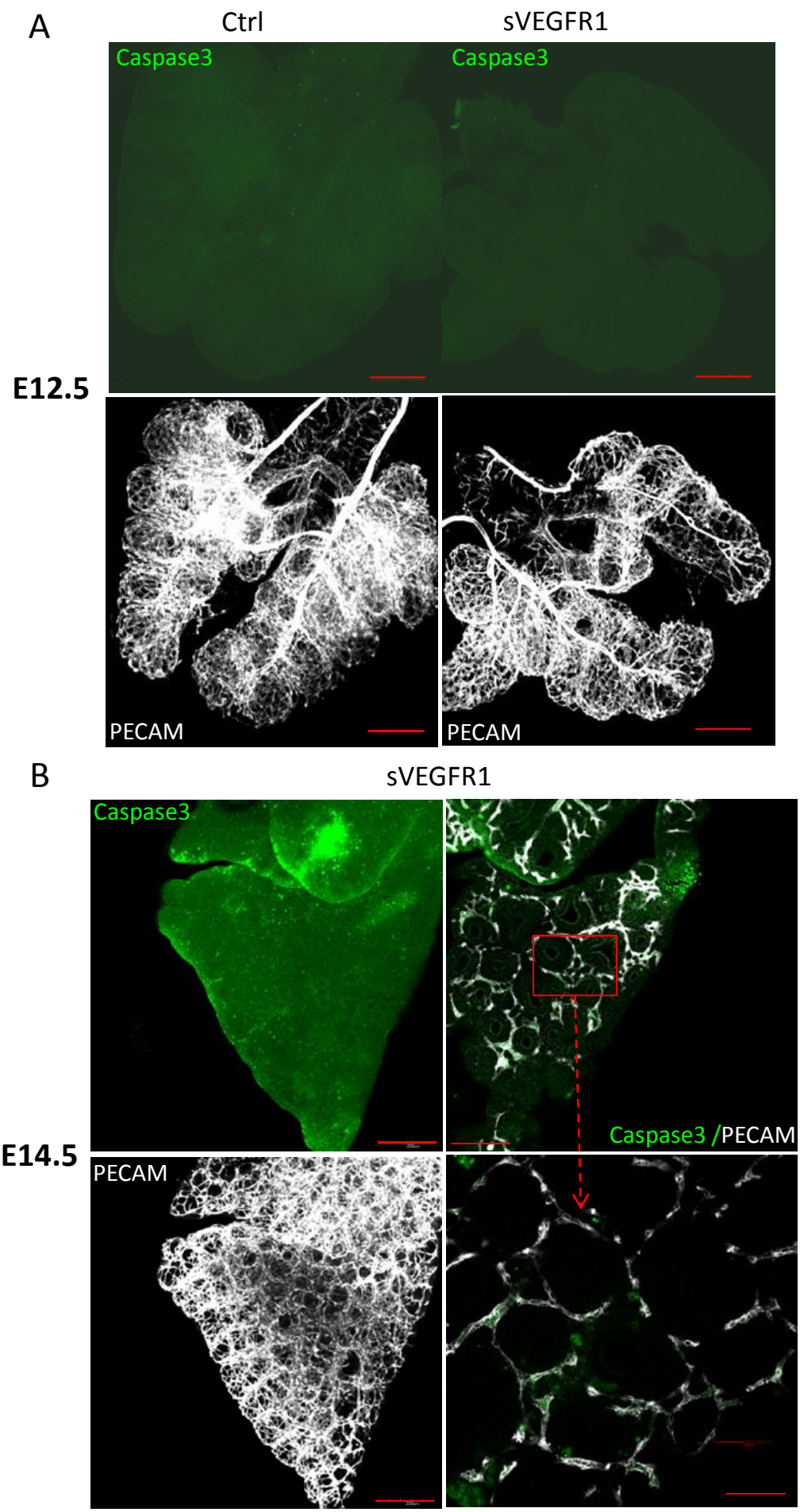
A
Ctrl
sVEGFR1
Caspase3
Caspase3
E12.5
PECAM
PECAM
B
sVEGFR1
Caspase3
Caspase3 /PECAM
E14.5
PECAM

A

Ctrl

sVEGF-R1

E12.5

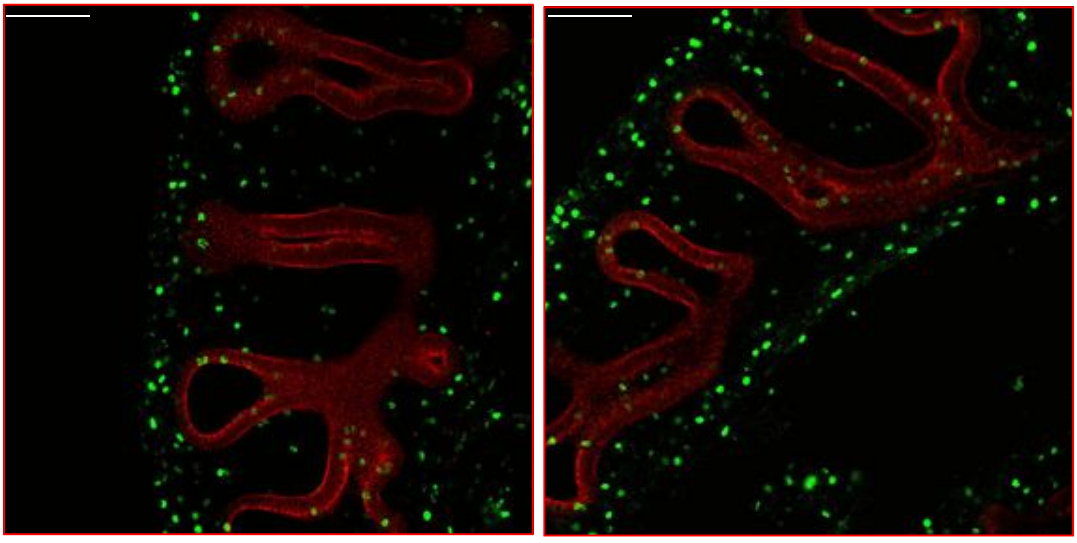

B

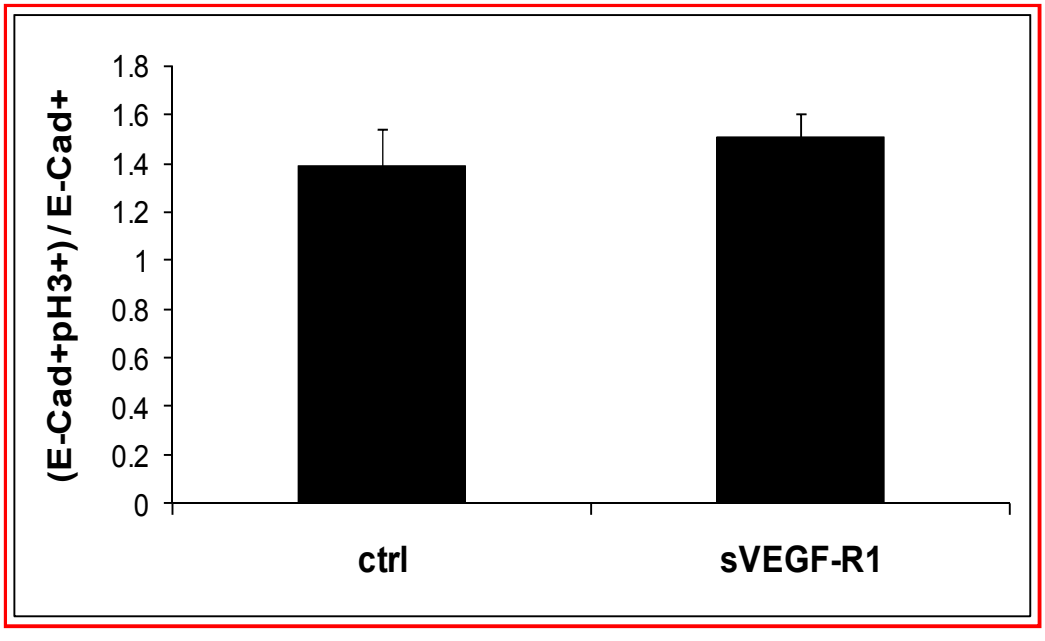

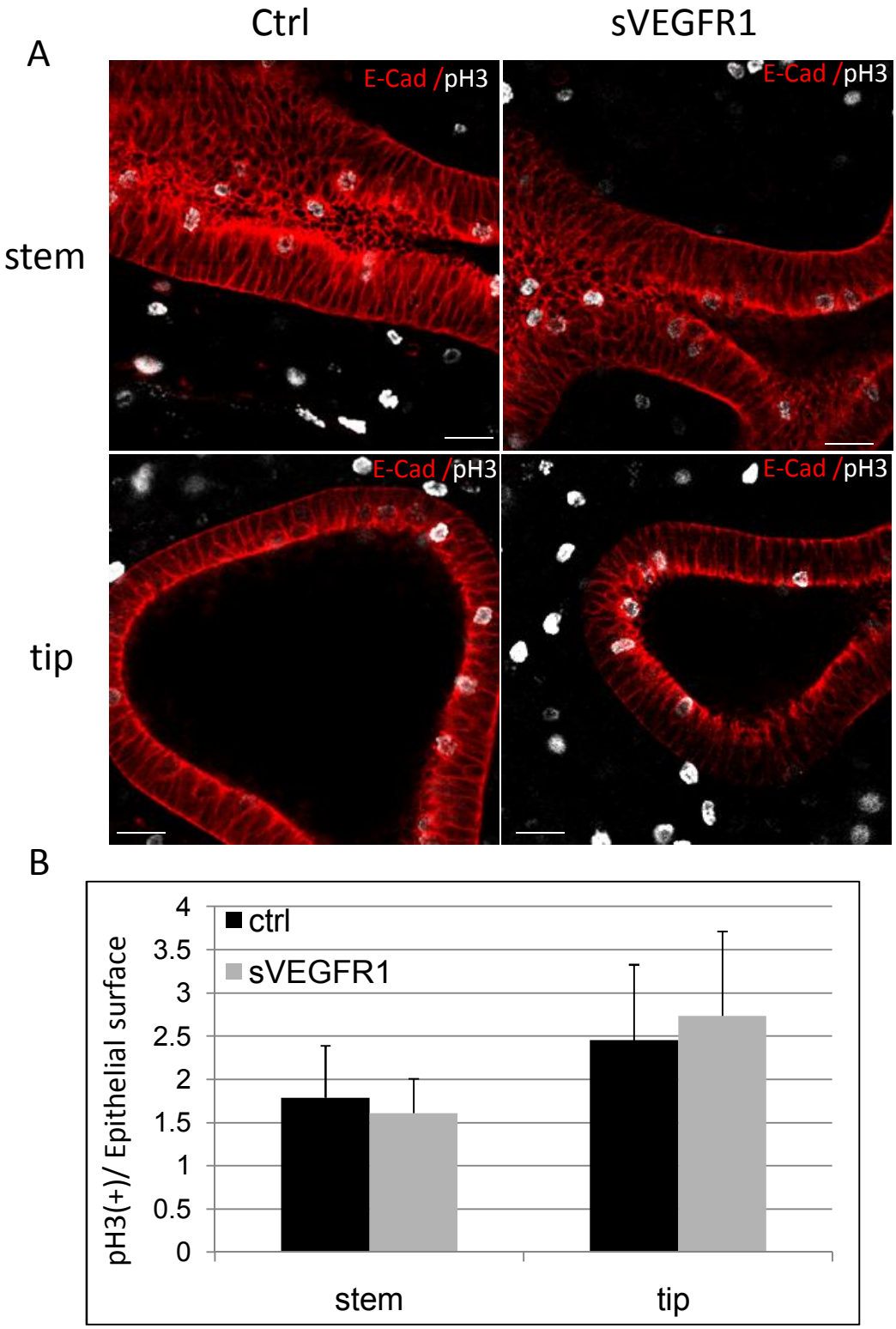
A
Ctrl
sVEGFR1
stem
tip
E-Cad /pH3
E-Cad /pH3
E-Cad /pH3
E-Cad /pH3
B
pH3(+)/ Epithelial surface
ctrl
sVEGFR1
4
3.5
3
2.5
2
1.5
1
0.5
0
stem
tip

A

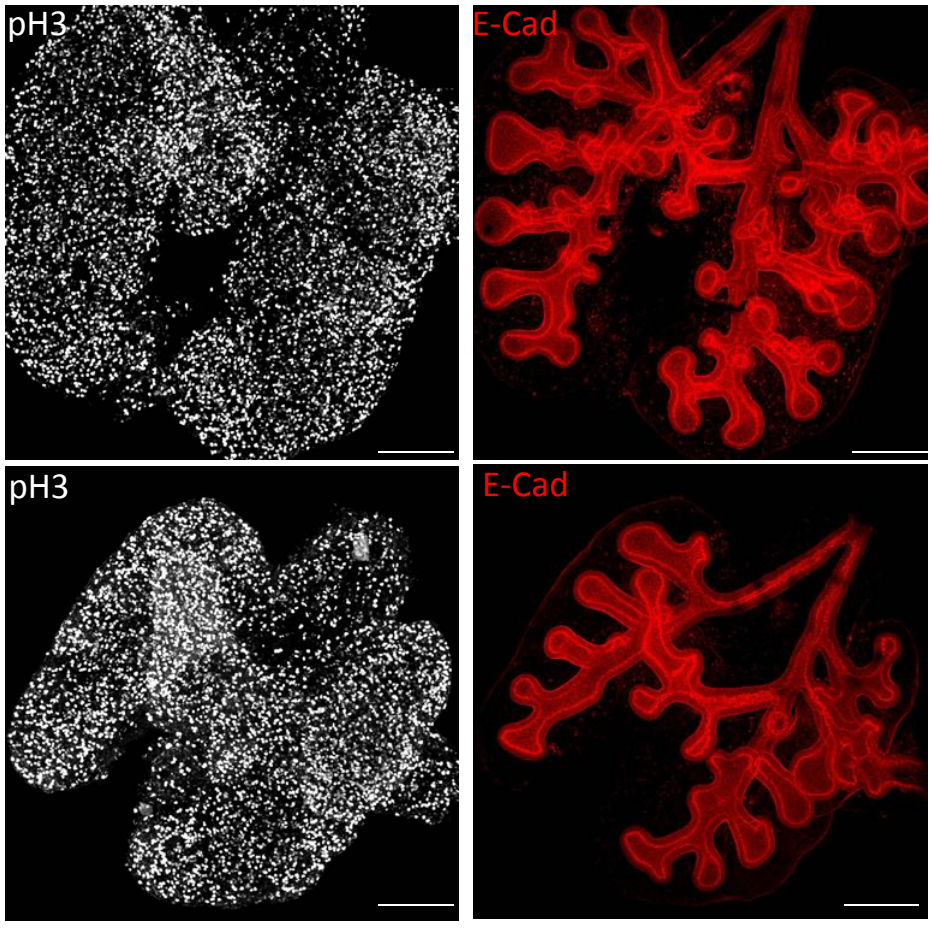
pH3
E-Cad
ctrl
pH3
E-Cad
sVEGFR1

B

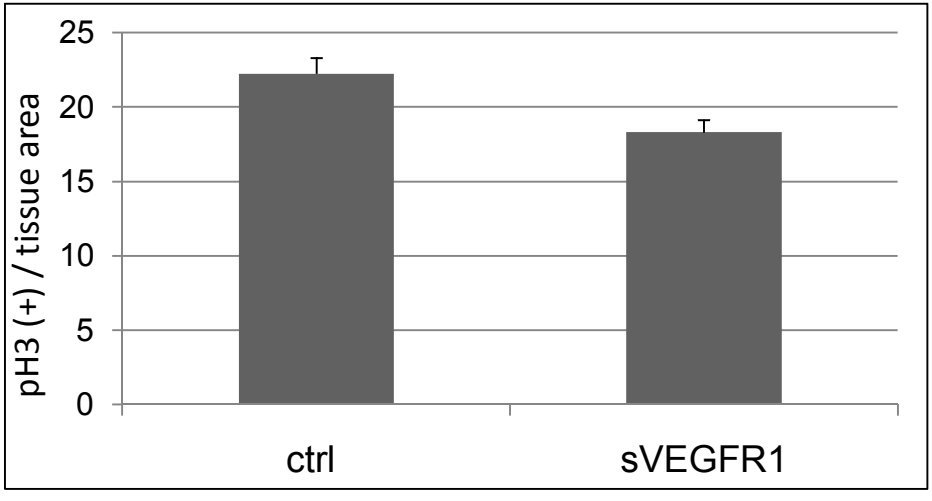
pH3 (+) / tissue area
25
20
15
10
5
0
ctrl
sVEGFR1

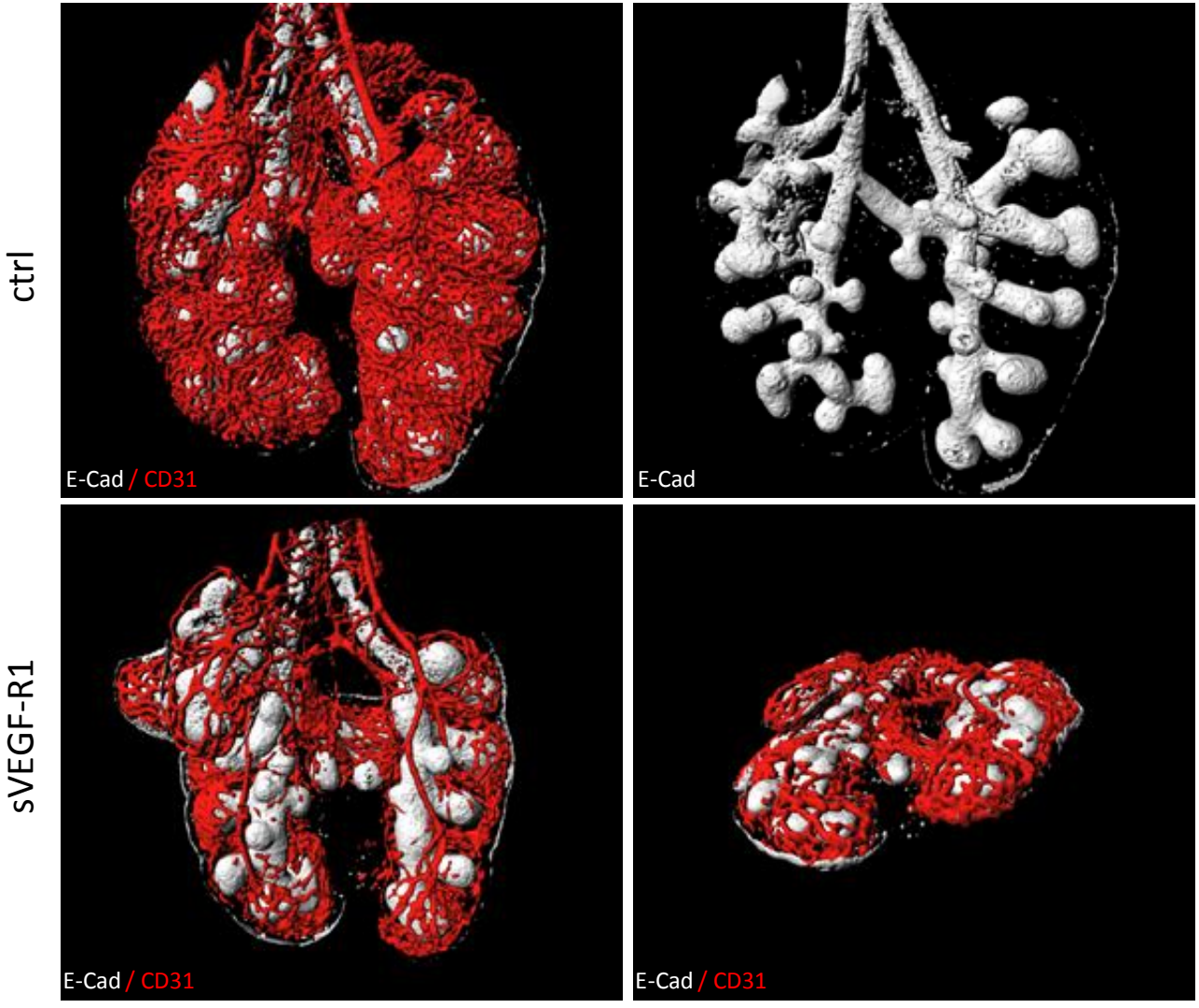
E12.5
ctrl
sVEGF-R1
E-Cad / CD31
E-Cad
E-Cad / CD31
E-Cad / CD31

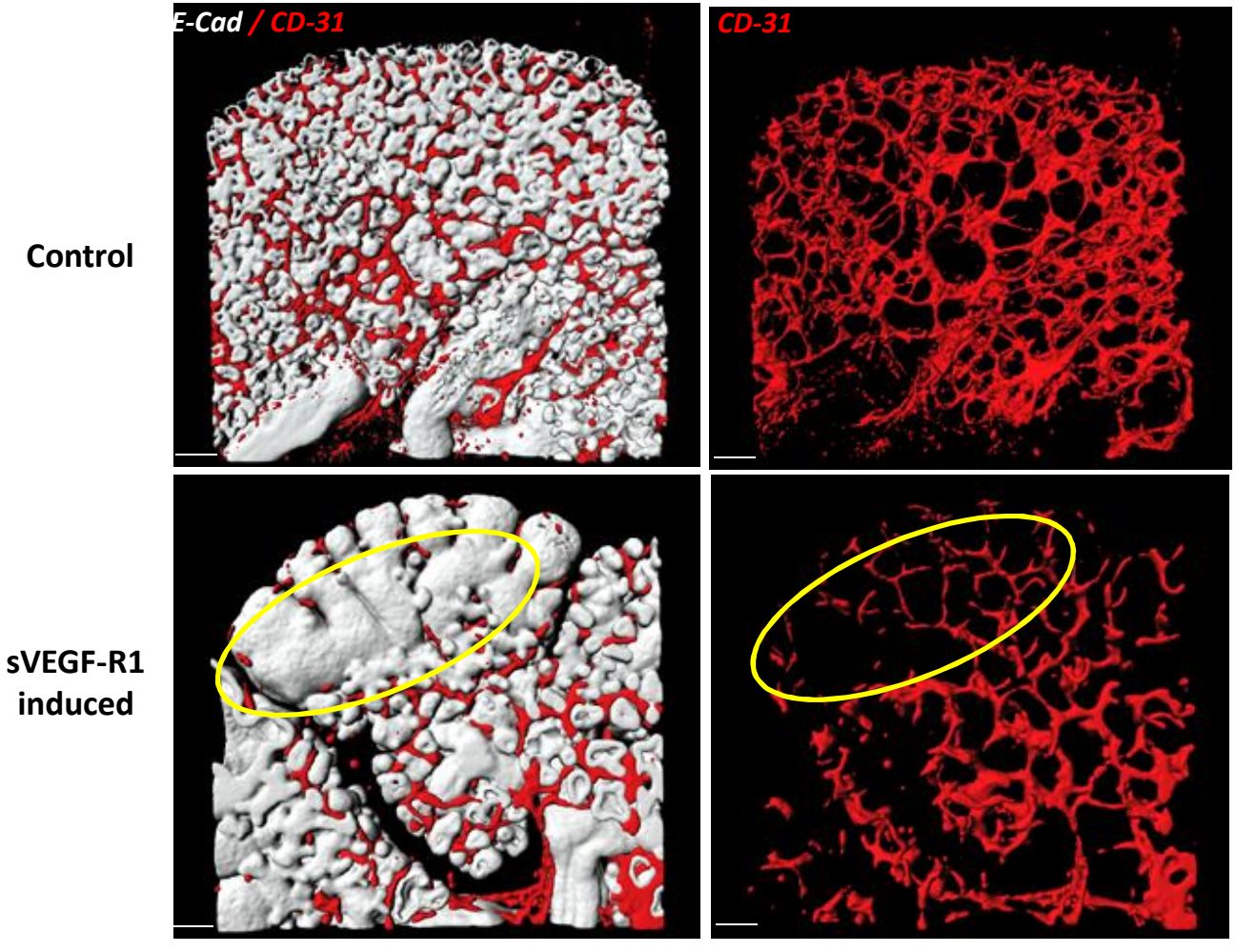
E-Cad / CD-31
CD-31
Control
sVEGF-R1
induced

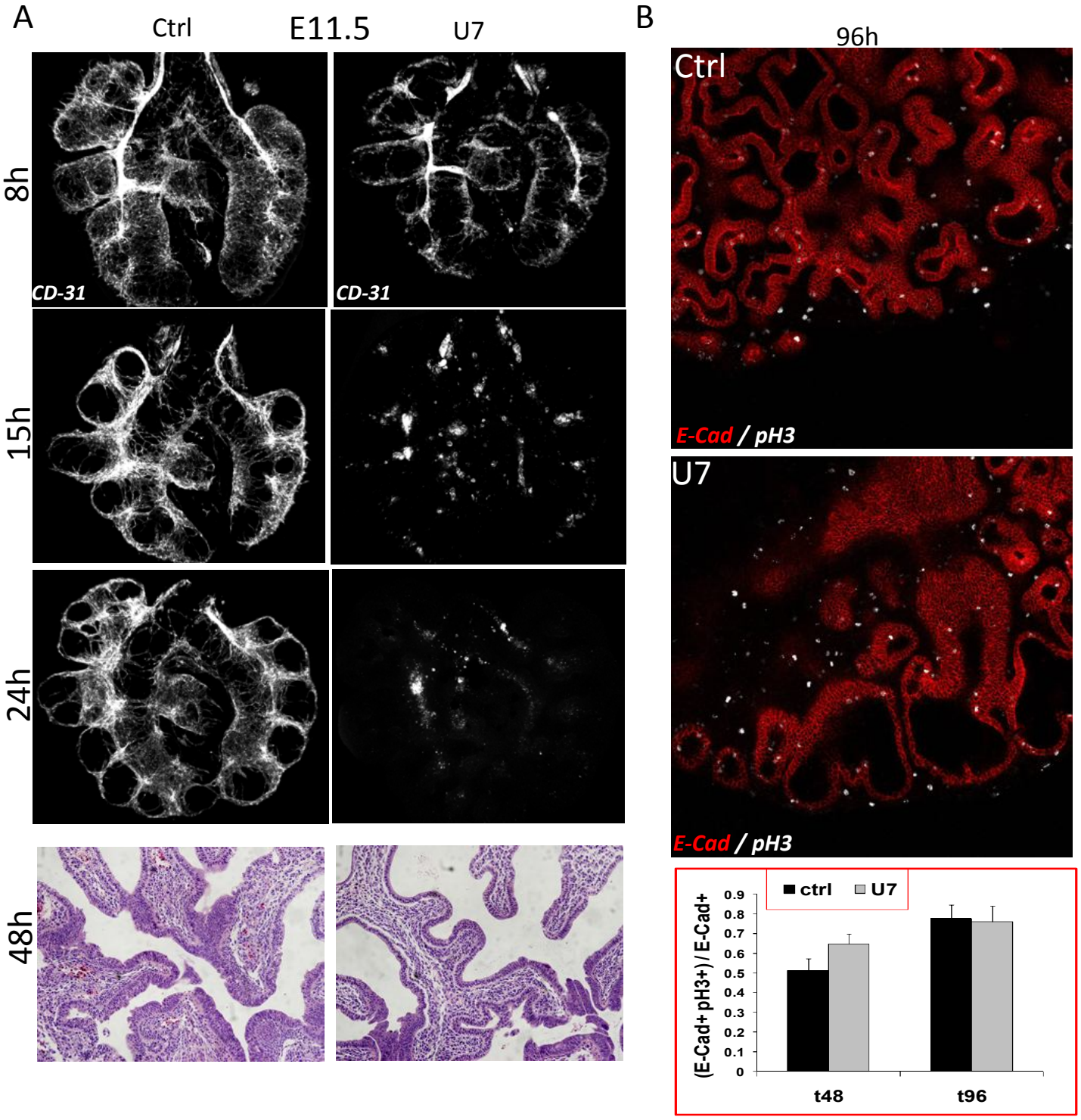
A
Ctrl
E11.5
U7
8h
15h
24h
48h
CD-31
CD-31
B
96h
Ctrl
E-Cad / pH3
U7
E-Cad / pH3
ctrl
U7
(E-Cad+ pH3+) / E-Cad+
0.9
0.8
0.7
0.6
0.5
0.4
0.3
0.2
0.1
0
t48
t96

Fig S10C,D

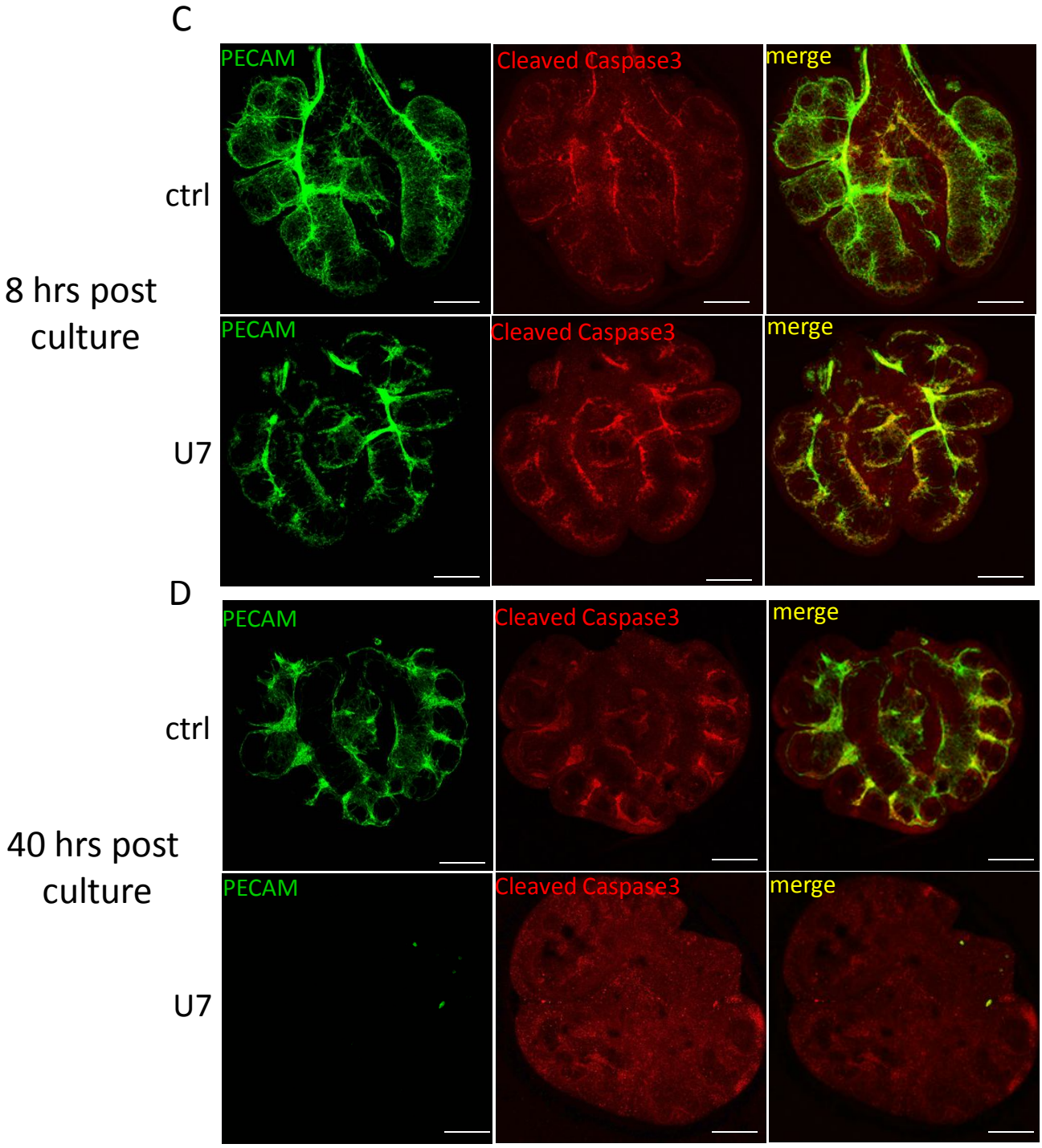
C
PECAM
Cleaved Caspase3
merge
ctrl
8 hrs post culture
PECAM
Cleaved Caspase3
merge
U7
D
PECAM
Cleaved Caspase3
merge
ctrl
40 hrs post culture
PECAM
Cleaved Caspase3
merge
U7

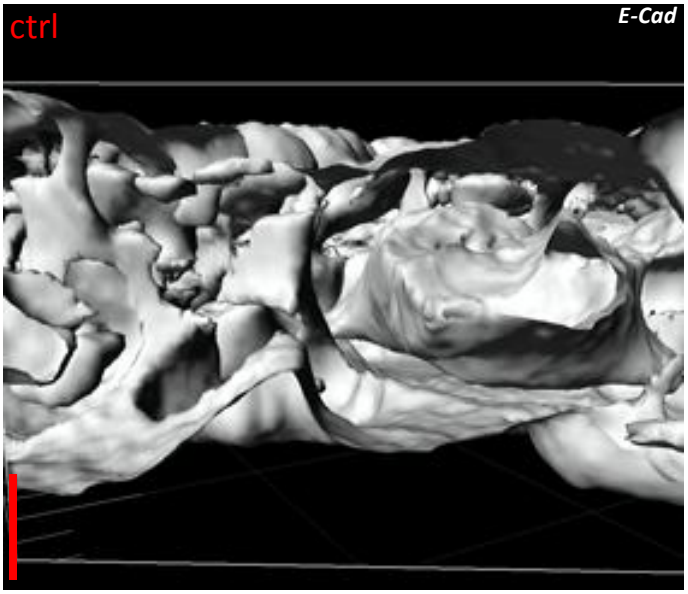
ctrl
E-Cad

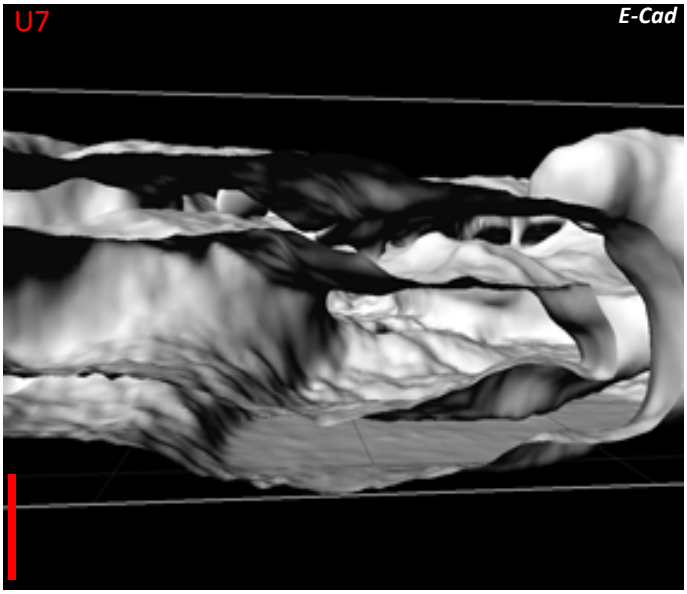
U7
E-Cad

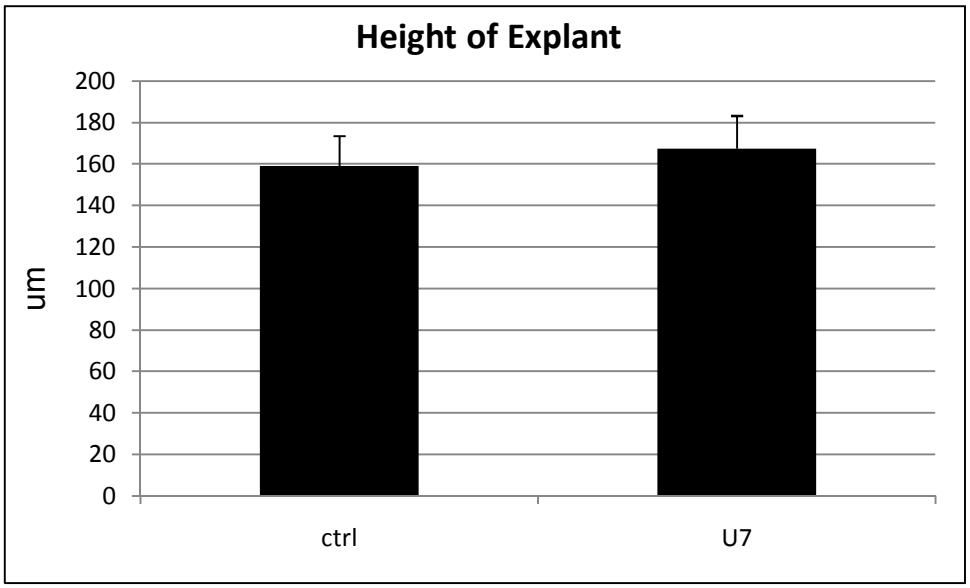
Height of Explant
um
200
180
160
140
120
100
80
60
40
20
0
ctrl
U7

A

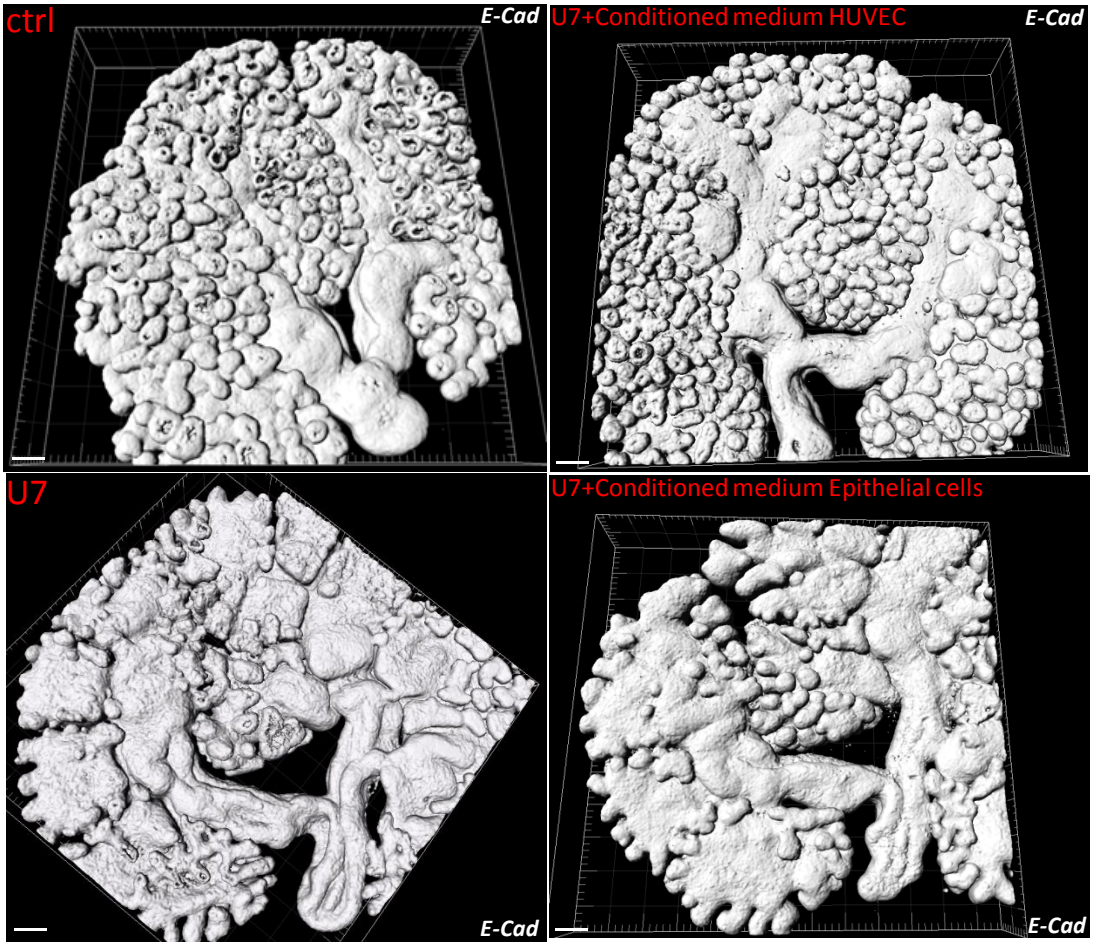
ctrl
E-Cad
U7+Conditioned medium HUVEC
E-Cad
U7
E-Cad
U7+Conditioned medium Epithelial cells
E-Cad

B

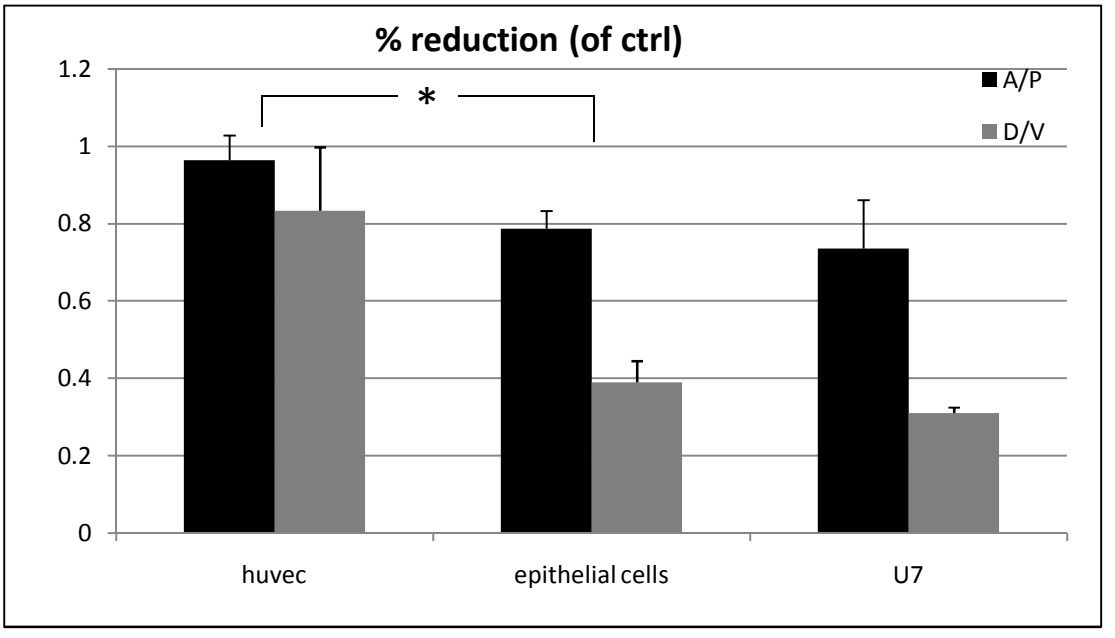
% reduction (of ctrl)
1.2
1
0.8
0.6
0.4
0.2
0
*
A/P
D/V
huvec
epithelial cells
U7

E12.5